OXFORD

# Activation of the cGAS-STING innate immune response in cells with deficient mitochondrial topoisomerase TOP1MT

Iman Al Khatib[1], Jingti Deng[1], Yuanjiu Lei[2], Sylvia Torres-Odio[2], Gladys R. Rojas[3], Laura E. Newman[3], Brian K. Chung[4,5],

Andrew Symes[6], Hongliang Zhang[7], Shar-yin N. Huang[7], Yves Pommier[7], Aneal Khan[8,9,10], Gerald S. Shadel[3], Andrew Phillip West[2],

William T. Gibson[11] and Timothy E. Shutt[12,*]

[1]Department of Biochemistry & Molecular Biology, Cumming School of Medicine, Alberta Children's Hospital Research Institute, University of Calgary, Calgary, Alberta T2N 4N1, Canada
[2]Department of Microbial Pathogenesis and Immunology, School of Medicine, Texas A&M University, Bryan, TX, USA
[3]The Salk Institute for Biological Studies, La Jolla, CA, USA
[4]Norwegian PSC Research Center, Oslo University Hospital, Rikshospitalet, Oslo, Norway
[5]Institute of Clinical Medicine, University of Oslo, Oslo, Norway
[6]Department of Geomatics Engineering, Schulich School of Engineering, University of Calgary, Calgary, Alberta T2N 1N4, Canada
[7]Laboratory of Molecular Pharmacology, Developmental Therapeutics Branch, Center for Cancer Research, NCI, National Institutes of Health, Bethesda, MD 20892, USA
[8]Discovery DNA, Calgary, Alberta T2L 1Y8, Canada
[9]M.A.G.I.C. Clinic Ltd. (Metabolics and Genetics in Calgary)
[10]Department of Pediatrics, Cumming School of Medicine, University of Calgary, Alberta Children's Hospital Research Institute, Calgary, Alberta T2M OL6, Canada
[11]Department of Medical Genetics, Faculty of Medicine,  British Columbia Children's Hospital Research Institute, University of British Columbia, Vancouver, British Columbia V5Z 4H4, Canada
[12]Departments of Medical Genetics and Biochemistry & Molecular Biology, Cumming School of Medicine, Alberta Children's Hospital Research Institute, Hotchkiss Brain Institute, Snyder Institute for Chronic Diseases, University of Calgary, Calgary, Alberta T2N 4N1, Canada

*To whom correspondence should be addressed. Tel: 403-220-6114; Email: timothy.shutt@ucalgary.ca

## Abstract

The recognition that cytosolic mitochondrial DNA (mtDNA) activates cyclic GMP–AMP synthase-stimulator of interferon genes (cGAS-STING) innate immune signaling has unlocked novel disease mechanisms. Here, an uncharacterized variant predicted to affect TOP1MT function, P193L, was discovered in a family with multiple early onset autoimmune diseases, including Systemic Lupus Erythematosus (SLE). Although there was no previous genetic association between *TOP1MT* and autoimmune disease, the role of TOP1MT as a regulator of mtDNA led us to investigate whether TOP1MT could mediate the release of mtDNA to the cytosol, where it could then activate the cGAS-STING innate immune pathway known to be activated in SLE and other autoimmune diseases. Through analysis of cells with reduced TOP1MT expression, we show that loss of TOP1MT results in release of mtDNA to the cytosol, which activates the cGAS-STING pathway. We also characterized the P193L variant for its ability to rescue several TOP1MT functions when expressed in *TOP1MT* knockout cells. We show that the P193L variant is not fully functional, as its re-expression at high levels was unable to rescue mitochondrial respiration deficits, and only showed partial rescue for other functions, including repletion of mtDNA replication following depletion, nucleoid size, steady state mtDNA transcripts levels and mitochondrial morphology. Additionally, expression of P193L at endogenous levels was unable to rescue mtDNA release-mediated cGAS-STING signaling. Overall, we report a link between TOP1MT and mtDNA release leading to cGAS-STING activation. Moreover, we show that the P193L variant has partial loss of function that may contribute to autoimmune disease susceptibility via cGAS-STING mediated activation of the innate immune system.

## Introduction

The innate immune response is the first line of defense against various microorganisms and pathogens. However, the immune system sometimes recognizes intracellular components as foreign and attacks its own tissue and organs, leading to autoimmune diseases. The exact cause for such erroneous autoimmune responses is not always understood, as there are many triggers that can lead to the self-reactivity of the immune system. Systemic lupus erythematosus (SLE) is a chronic, heterogenous, systemic autoimmune disease, in which accumulating evidence suggests that mitochondrial dysfunction plays an important role

(1,2). Multiple genetic variants, including highly penetrant rare variants, have been associated with SLE susceptibility. The identification and functional characterization of such rare variants can provide significant insight into the cause, mechanisms and potential treatment options for patients (3–6).

Mitochondria, best known as the powerhouses of the cell, are eukaryotic organelles that evolved from prokaryotes through an endosymbiotic event that occurred billions of years ago (7). The strongest evidence for their bacterial origin is the fact that mitochondria have retained their own 16 569 bp circular genome, the mitochondrial DNA (mtDNA), which is present in hundreds

to thousands of copies in the cell (8). Release of mtDNA into the cytosol, in response to pathogen-induced mitochondrial stress, is a mechanism by which cells can amplify innate immune signaling in response to pathogen invasion (9,10). However, in the absence of pathogens, mitochondrial dysfunction can also cause release of mtDNA into the cytosol, leading to 'sterile' activation of the innate immune system (11–13). The mechanism of release of mtDNA into the cytosol has been studied primarily in the context of apoptosis through BAK/BAX protein pores (14). However, another mechanism of mtDNA release has been described that depends on the opening of mitochondrial permeability transition pores in the inner mitochondrial membrane (15), and oligomerization of voltage-dependent anion channel (VDAC) in the mitochondrial outer membrane (16). Although less is known about when and how mtDNA is released under more physiological conditions, there is a growing appreciation of the functional consequences with respect to inflammation and disease. Recent research has demonstrated that release of mtDNA into the cytosol can activate innate immune pathways mediated by Toll-like receptor 9, the Nod-like receptor protein 3 inflammasome, and of particular relevance here, the cyclic GMP–AMP synthase-stimulator of interferon genes (cGAS-STING) pathway (17).

The cGAS-STING pathway is an immune response that recognizes cytosolic DNA, which can come from a variety of sources including the mitochondria (18–20). Upon binding to DNA, cGAS dimerizes and becomes activated, whereupon it catalyzes the synthesis of cyclic dinucleotide cGAMP ($2'3'$ cyclic GMP–AMP) from adenosine triphosphate (ATP) and guanosine triphosphate (GTP). These cGAMP dinucleotides then bind STING, causing conformational changes that lead to STING oligomerization and subsequent translocation from the endoplasmic reticulum (ER) to the Golgi apparatus (21,22). This activated STING recruits TANK-binding kinase 1 (TBK-1) (17), which causes a series of events leading to phosphorylation of interferon regulatory factor 3 (IRF3). In turn, the phosphorylated IRF3 translocates to the nucleus where it induces expression of type I interferons, interferon-stimulated genes (ISGs), and several other inflammatory mediators, pro-apoptotic genes and chemokines (21).

The first work linking mtDNA to the cGAS-STING pathway showed that depletion of the mitochondrial DNA packaging protein TFAM led to cytosolic release of mtDNA, resulting in cGAS-STING activation (23). More recently, deficiency in the mitochondrial CLPP (Caseinolytic mitochondrial matrix peptidase proteolytic subunit) protease subunit was also shown to result in mtDNA instability and activation of type I IFN signaling through cGAS-STING (24). Meanwhile, cytosolic mtDNA release (25) and activation of cGAS-STING have also been implicated in Parkinson disease (26). Many inflammatory diseases also show activation of cGAS-STING in damaged organs, like liver (27–29), kidney (30,31) and pancreas (32). The involvement of TFAM and CLPP in mtDNA release into the cytosol and cGAS-STING activation raises the question of whether impairment of mtDNA maintenance caused by coding variants in other proteins might have similar consequences. One intriguing candidate is TOP1MT, a topoisomerase that helps resolve crossovers and knots that can originate during maintenance of the circular mtDNA genome. TOP1MT is the only human topoisomerase that is solely present in the mitochondria (33–35), where it plays important roles in mtDNA replication, transcription and translation (36–39). Interestingly, a wide range of autoantibodies have been described and detected in the serum of SLE patients (40,41), including anti-double-stranded DNA (anti-dsDNA) (42,43) and autoantibodies recognizing the nuclear

topoisomerase enzyme TOP1 (44–47) as well as the mitochondrial TOP1MT (48).

Here, we characterize a Variant of Unknown Significance in TOP1MT, P193L, identified in a family with several members who presented with SLE and a variety of other autoimmune disorders. Notably, activation of the cGAS-STING pathway is linked to SLE (49,50). For example, an activating mutation in STING causes lupus-like manifestations (51). To date, the connection between cGAS-STING activation in SLE has only been noted in the context of nuclear DNA present in the cytosol (50,52). Meanwhile, inhibition of VDAC-mediated cytosolic mtDNA release was beneficial in a mouse model of SLE (16), suggesting a role for cytosolic mtDNA in promoting SLE. Here, we uncover a novel connection between TOP1MT dysfunction and activation of the cGAS-STING pathway via mtDNA, which may contribute to the autoimmune phenotypes in several members of this family, and provide further evidence for the potential role of mtDNA in the pathogenesis of autoimmune disorders.

## Results

The family was originally ascertained on the basis of congenital leptin deficiency in the index patient's daughter (53). However, the proband for the lupus phenotype, III-8 (the mother), has been diagnosed with hypothyroidism, SLE, Sjogren's syndrome, fibromyalgia with peripheral neuropathy. Now in her mid-50s, she has moderate to severe pulmonary fibrosis. She is thought to have celiac disease as well, though the latter is not biopsy-proven. As seen in the extended family pedigree (Supplementary Material, Fig. S1), multiple family members were diagnosed with autoimmune diseases. One of the proband sisters, III-13 (from a sibship of eight), was diagnosed with lupus at age 30 years, and one of her nieces, V-6 (the daughter of one of her brothers), was diagnosed with rheumatoid arthritis in her late teens. The proband husband, III-7, is clinically unaffected, though his sister, III-5, was diagnosed with polyarthritis in her 40s, and one of her daughters, IV′- 2, was diagnosed with lupus at age 14 years and died at age 24 years. Furthermore, another of her daughters, IV′-4, was diagnosed with rheumatoid arthritis in infancy. Attempts to collect and analyze DNA on these individuals have not yet been successful. Additional clinical information on the nuclear family is available in supplemental information (Supplementary Material, File S1).

## Variant identification

Chromosomal microarray studies did not identify any microdeletions or microduplications that met clinical criteria for being considered pathogenic or likely pathogenic. Exome sequencing in members of the proband's nuclear family did not identify any known pathogenic variants in recognized Mendelian disorders. However, TOP1MT was flagged as a potential genetic cause of monogenic SLE when a P193L missense variant was discovered in the consanguineous family, with multiple members affected by pediatric-onset autoimmune disease, including SLE (Fig. 1A). The P193L variant is a result of a point mutation at cDNA position 578C > T (NM_052963.2) that results in a proline to leucine change at amino acid 193, which is predicted to be possibly damaging and deleterious with minor allele frequency (MAF) of 0.00002786 in Genome Aggregation Database v2.1.1, and a MAF of 0.0001307 within the South Asian superpopulation sampled by v2.1.1. The identified variant occurs at a highly conserved site in the core domain of TOP1MT (Fig. 1B), which is located within the DNA binding barrel (Fig. 1C).
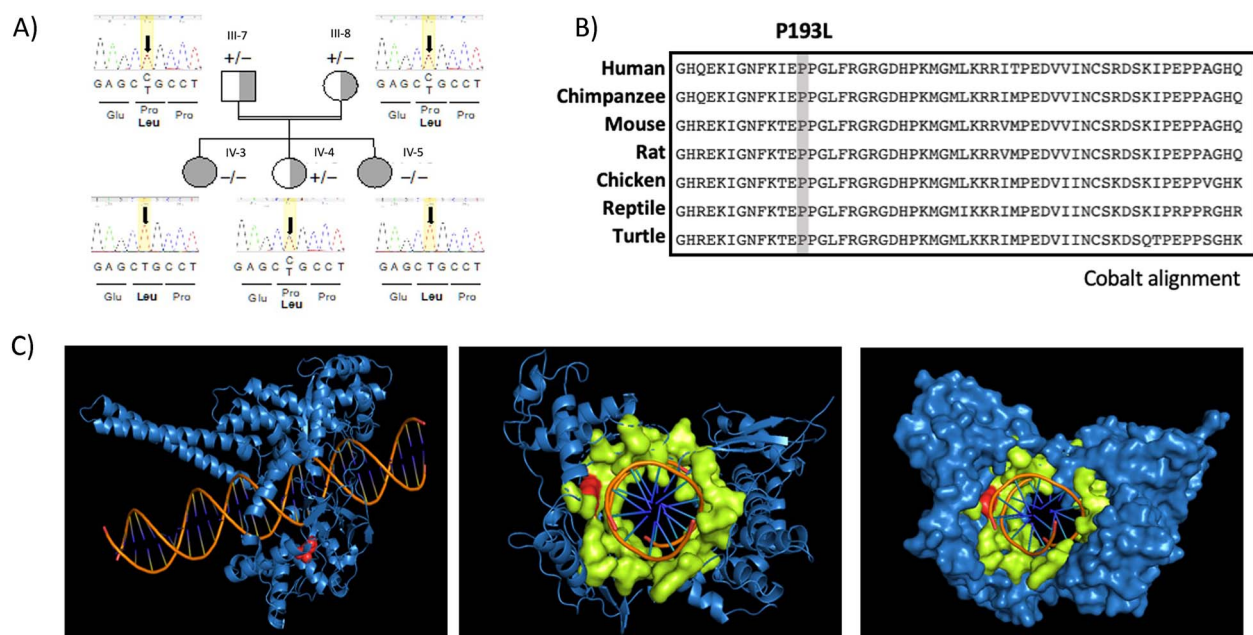
**Figure 1.** Family with the P193L TOP1MT variant and protein structure. (**A**) Pedigree of the proband's nuclear family indicating the P193L genotype; the sequences show the nucleotide identity at position C578T where a missense Pro193Leu TOP1MT alteration was found. An extended family pedigree can be found in Supplementary Material, Figure S1. (**B**) Amino acid alignments of TOP1MT proteins from a variety of vertebrate species generated using COBALT shows the conservation of the amino-acid variant identified in the affected family. (**C**) Structural modeling of the TOP1MT protein bound to double-stranded DNA. Residues in the nucleic acid binding barrel are shown in lime, with the modeled P193L variant shown in red.

Preliminary functional studies in patient-derived white blood cells from family members that were either heterozygous or homozygous for the P193L variant showed impaired oxidative phosphorylation (OxPhos) (Supplementary Material, Fig. S2) compared with healthy controls, suggestive of underlying mitochondrial dysfunction. However, additional work was necessary to confirm whether the P193L variant impacts the functionality of TOP1MT, and to investigate potential mechanisms that might link TOP1MT to SLE.

## TOP1MT depletion leads to cytosolic mtDNA release and activation of cGAS-STING signaling

Given the SLE and other autoimmune disease phenotypes in the family, and the role of TOP1MT as a mediator of mtDNA, we hypothesized that TOP1MT dysfunction could contribute to cytosolic release of mtDNA and activation of the cGAS-STING pathway. To investigate this notion, we took advantage of HCT116 cells wherein *TOP1MT* is knocked out via CRISPR-Cas9 (54). We first measured the abundance of mtDNA present in cytosol extracts. Using several primer sets that amplify distinct regions of the mtDNA, quantitative PCR consistently detected significantly higher levels of mtDNA in the cytosol extracts of HCT116 *TOP1MT* KO cells (HCT116 KO) compared with HCT116 wild-type (HCT116 WT) (Figs 2A). Fluorescence *in situ* hybridization (FISH) also confirmed higher levels of cytosolic mtDNA in HCT116 KO cells compared with HCT116 WT (Figs 2B and C). Moreover, the cytosolic mtDNA in HCT116 KO cells co-localized with cGAS (Figs 2B and D), implicating the cGAS-STING innate immune pathway.

Next, to see if the increased cytosolic mtDNA activated cGAS-STING signaling, we examined the expression of type I interferons. Consistent with activation of the cGAS-STING signaling pathway, both interferon-alpha (IFN-$\alpha$) and interferon-beta (IFN-$\beta$) were elevated in HCT116 KO cells. However, levels of the type II interferon-gamma (IFN-$\gamma$), which is not regulated by cGAS-STING, were not altered (Fig. 2E). As there are multiple

activators of innate immune responses, we wanted to confirm that this type I interferon elevation occurred through the cGAS-STING pathway. To this end, 24 h treatment of cells with RU.521, an inhibitor of cGAS (55), led to lower interferon levels among HCT116 KO cells, whereas basal levels in HCT116 WT cells remained unchanged (Figs 2F and G). Subsequently, upon removal of RU.521, the interferon levels were further elevated again in HCT116 KO cells relative to HCT116 WT controls (Fig. 2H). Collectively, these novel findings suggest that loss of TOP1MT results in increased levels of cytosolic mtDNA, and increased cGAS-STING dependent expression of IFN-$\alpha$ and IFN-$\beta$ transcripts.

Although we saw a significant increase in cGAS-dependent levels of IFN-$\alpha$ and IFN-$\beta$ in HCT116 cells, this increase was relatively mild compared with a typical type I interferon response during viral infection, likely because of the fact that HCT116 cells are a cancer cell line and have been reported to be hypo-responsive to cGAS-STING pathway activation (56,57). Thus, we wanted to confirm our findings in additional cells lines. To this end we knocked down TOP1MT via small interfering RNA (siRNA) in telomerase immortalized human fibroblasts (Supplementary Material, Fig. S3a), as well as in mouse embryonic fibroblasts (MEFs) (Supplementary Material, Fig. S3b). We observed a significant increase in several ISGs (e.g. Cxcl10, Ifit1, Ifit3) in human fibroblasts, grown at either 20% oxygen (Fig. 3A) or 3% oxygen (Fig. 3B), as well as in MEFs (Fig. 3C). Consistent with this elevation of ISGs being dependent on cGAS-STING signaling, cGAS$^{-/-}$ MEFs did not show the same strong elevation of ISG levels upon TOP1MT depletion (Fig. 3C). Together, these findings identify a novel role for TOP1MT in mediating mtDNA release and activation of cGAS-STING innate immunity.

## Generation of TOP1MT rescue cell lines

Given the mitochondrial dysfunction noted in patient-derived blood cells (Supplementary Material, Fig. S2), we examined the ability of the TOP1MT P193L variant to rescue multiple
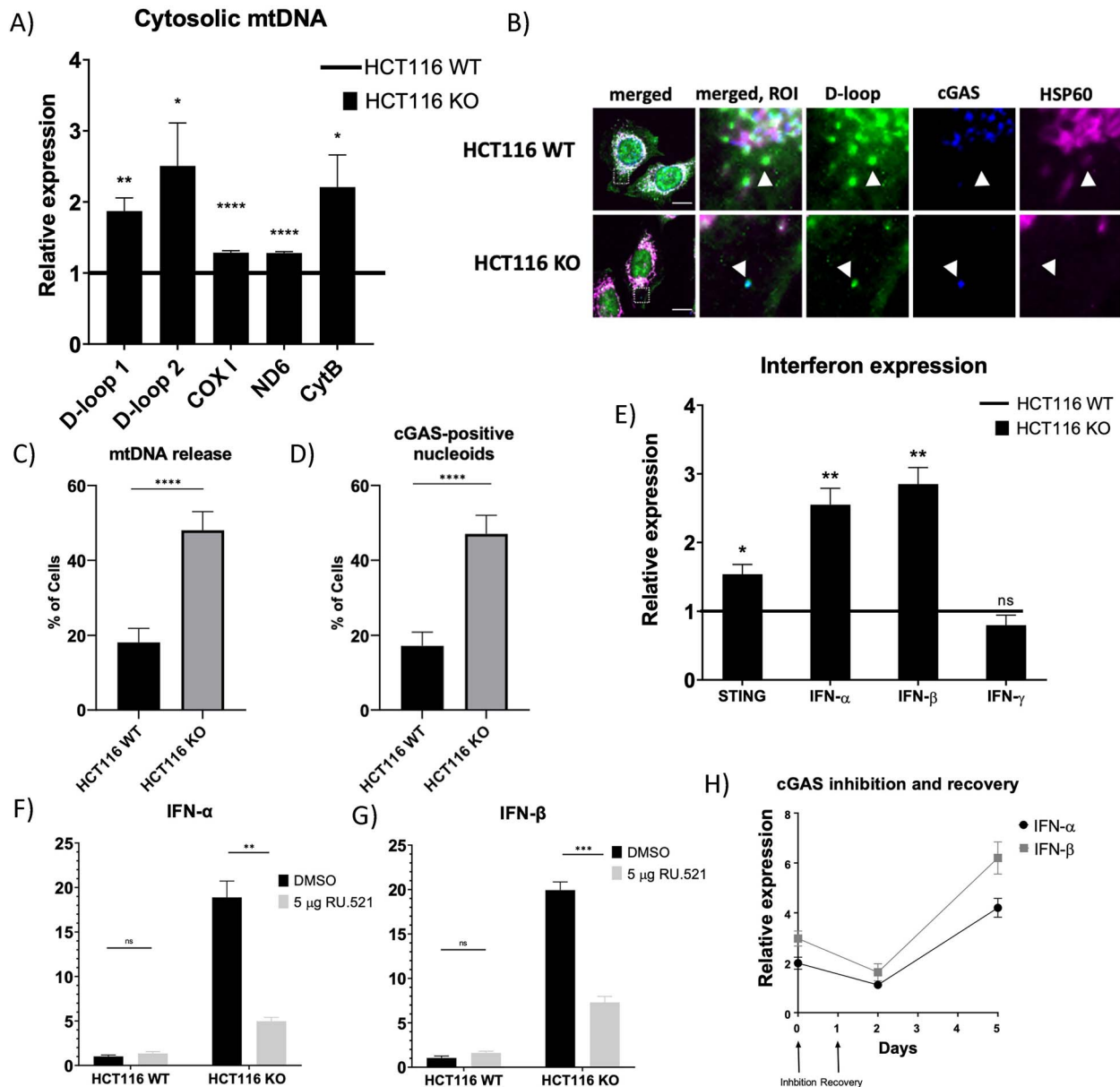
**Figure 2.** Elevated cytosolic mtDNA release and cGAS-STING pathway activation in TOP1MT KO cells. (**A**) Cytosolic mtDNA was quantitated via qPCR using the indicated primer sets and was found to be elevated in TOP1MT KO cells compared with WT cells. Normalization was done relative to the corresponding amplicons in total DNA. (**B**) Confocal images of mtDNA FISH (D-loop probe, green), followed by immunofluorescence against cGAS (blue) and HSP60 (magenta). Scale bar = 10 um. (**C**) Quantification of the number of cells with non-mitochondrial nucleoids ($N = 105$ for HCT116 WT, $N = 102$ for HCT116 KO; pooled from three replicate experiments). (**D**) Quantification of number of cells exhibiting co-localization of non-mitochondrial nucleoids with cGAS, as in (b). (**E**) Real-Time Quantitative Reverse Transcription PCR (qRT-PCR) analysis of STING, type I and type II interferons expression in TOP1MT KO cells compared with WT cells. Inhibition of cGAS by 5 $\mu$g/ml RU.521 for 24 h lowers type I interferon expressions in TOP1MT-KO cells for both IFN-$\alpha$ (**F**) and IFN-$\beta$ (**G**), as measured by qRT-PCR. (**H**) Quantification of type I interferon levels by qRT-PCR in TOP1MT KO cells at the indicated times following 24 h treatment with 5 $\mu$g/ml RU.521 and recovery in fresh media. All statistical analysis were done using unpaired student $t$-test and P-values * $< 0.05$, ** $< 0.01$, *** $< 0.001$ and **** $< 0.0001$. 'ns' signifies no significant differences between indicated groups. Error bars represent standard error of mean.

mitochondrial parameters impaired in HCT116 KO cells (39). As described previously (39), starting from HCT116 WT and HCT116 KO, we generated four different stable cell lines using retroviral constructs expressing TOP1MT and the mCherry fluorescent protein separated by a self-cleavage peptide (TOP1MT-T2A-mCherry), or an empty vector control. This construct leads to expression of TOP1MT, which will be directed to the mitochondria by the mitochondrial targeting sequence, and mCherry, which can be used to monitor transduction. Two control cell lines, henceforth referred to as WT-ctrl and KO-ctrl, were generated by transducing

an empty vector expressing only mCherry in the HCT116 WT and HCT116 KO cells, respectively. A third cell line was generated by re-expressing wild-type TOP1MT (indicated as Rescue) in HCT116 KO cells. Finally, a fourth cell line expressing the patient variant P193L was also established (referred to as P193L).

The expression of mCherry was used to sort the positively transduced cells by flow cytometry. Transduction was further confirmed by PCR amplification of the inserted TOP1MT open reading frame (Fig. 4A), and DNA sequencing to confirm the identity of the Rescue and the P193L variant cell lines (Fig. 4B).
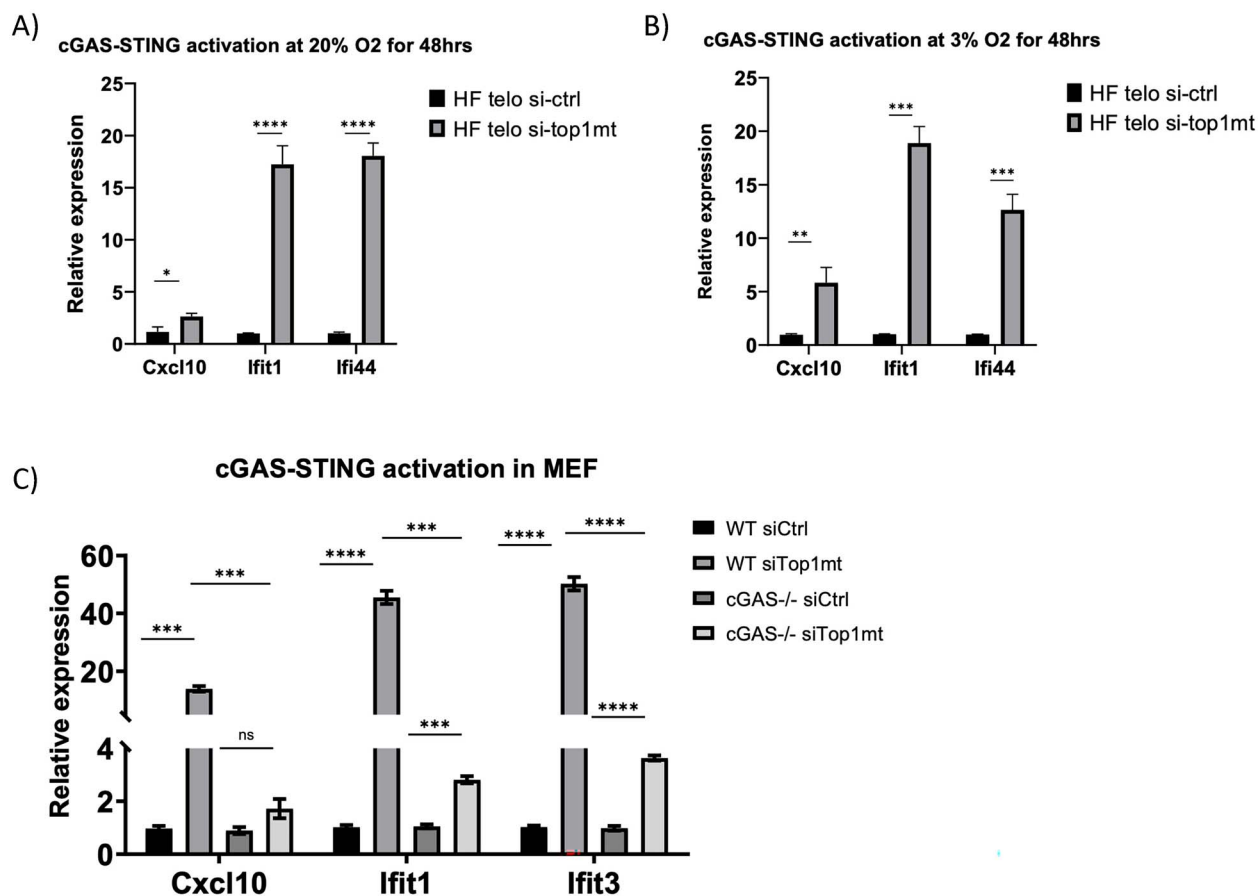
**Figure 3.** cGAS-STING pathway induction upon TOP1MT ablation in human and mouse fibroblasts. (**A**, **B**) siRNA knockdown of TOP1MT causes strong induction of ISGs, as measured by qRT-PCR, in telomerase immortalized human fibroblasts at both 20% (a) and 3% oxygen (b). (**C**) ISG expression measured by qRT-PCR is elevated in WT MEFs upon Top1mt knockdown, but this elevation is abrogated in cGAS knockout MEFs. All statistical analysis were done using unpaired student *t*-test and *P*-values * < 0.05, ** < 0.01, *** < 0.001 and **** < 0.0001. 'ns' signifies no significant differences between indicated groups. Error bars represent standard error of mean.

Next, immunoblotting was used to confirm the expression of TOP1MT proteins (Fig. 4C). A band of the predicted size of ~70 kDa corresponding to TOP1MT protein was observed WT-ctrl, Rescue and P193L cells, but not in the KO-ctrl cells (Fig. 4D). Notably, the levels of TOP1MT protein in the Rescue and P193L lines were ~10-fold higher than the endogenous TOP1MT protein levels in the WT-ctrl cells. Further validation of the protein expression was confirmed via immunofluorescence imaging, wherein overexpressed TOP1MT protein was detected, and confirmed to localize to mitochondria (Fig. 4E).

Next, we wanted to determine the ability of the P193L variant to rescue the aberrant functions previously identified in HCT116 KO cells (39), including: reduced nucleoid size, the hyperfused mitochondrial network, and decreases in mitochondrial transcription, mtDNA replication, mitochondrial translation and oxidative phosphorylation.

## Nucleoids

On the basis of our previous work (39), and the role of TOP1MT in preventing negative supercoiling of mtDNA (58) we examined mtDNA. To look at supercoiling, we used a southwestern blot approach that labels mtDNA with BrdU, which can then be separated on an agarose gel, transferred to a membrane and visualized by immunoblotting. To confirm which bands represent linear, relaxed or supercoiled mtDNA, DNA was treated with either BamHI or topoisomerase enzymes. Consistent with the expected

reduction of topoisomerase activity, we found that KO-ctrl cells had a higher ratio of supercoiled to relaxed mtDNA compared with WT-ctrl cells, and that this was reversed in the Rescue cells (Fig. 5A). Though the P193L line appeared to show increased supercoiling of mtDNA relative to the rescue line, the ratio of supercoiled mtDNA to the relaxed mtDNA was not significantly altered (Fig. 5B).

As an alternative approach to gain insight on the mtDNA topology, we quantified the size of individual nucleoids stained with PicoGreen using confocal microscopy (Fig. 5C). As expected, and consistent with the southwestern blot analysis showing increased supercoiling, mtDNA nucleoids were significantly smaller in KO-ctrl cells, and this was reversed by overexpression of the WT TOP1MT in the Rescue line. However, the overexpression of the P193L variant failed to fully rescue the nucleoid sizes (Fig. 5D) to the same level as the WT protein, suggesting that this variant has reduced topoisomerase activity.

## Mitochondrial morphology

The mitochondrial network is dynamic and can change in response to various physiological cues. In KO-ctrl cells, mitochondrial networks imaged by confocal microscopy were more fused than their WT-ctrl counterparts, and this was reversed by re-expression of the WT protein in the Rescue cells (Supplementary Material, Figs S4a and b). However, expression of the patient variant had an intermediate effect on mitochondrial morphology,
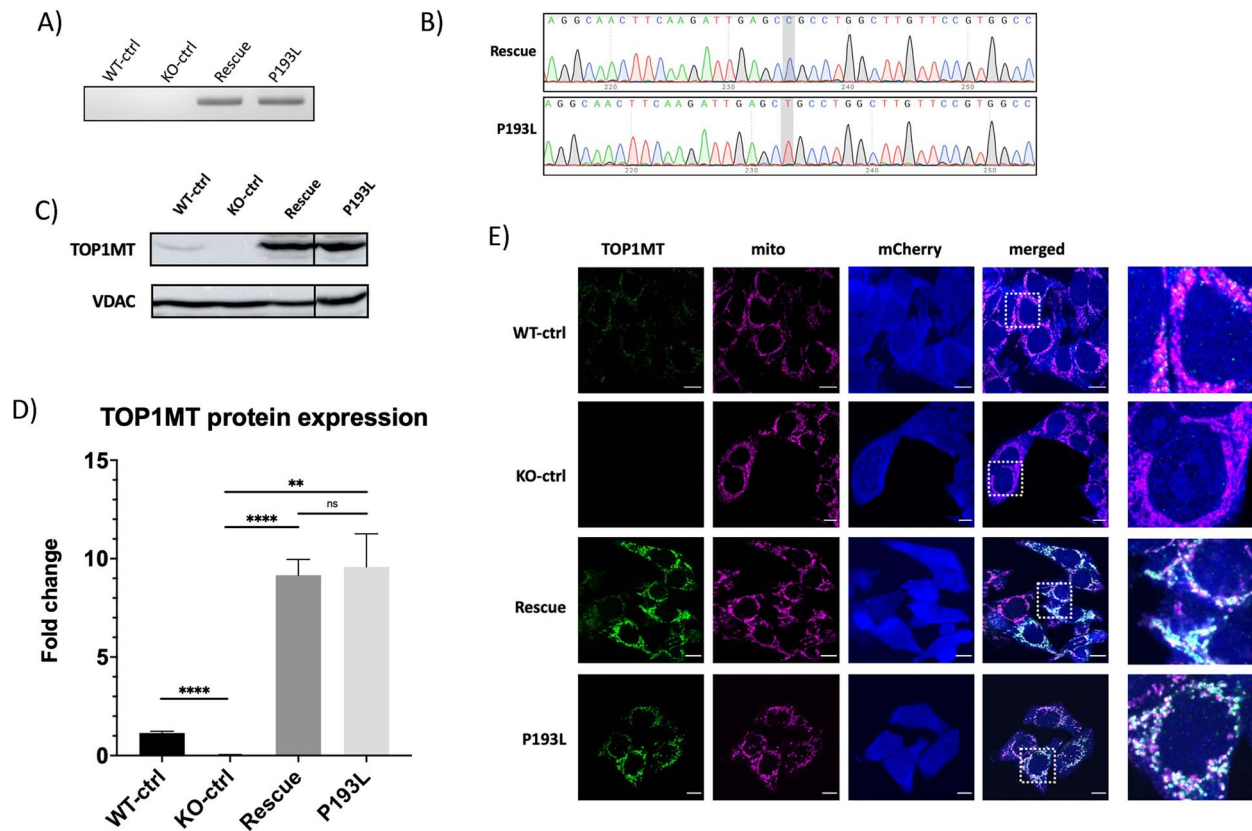
**Figure 4.** Generation of stable line expressing the variant form of TOP1MT. (**A**) PCR amplification targeting the coding region of the viral-encoded TOP1MT open reading frame, spanning patient variant, confirms amplicons are present only in HCT116 KO cell lines stably re-expressing TOP1MT, namely the Rescue and P193L lines. (**B**) Chromatograms from Sanger sequencing of the amplicons produced from (a). The 578C residues (shaded), confirm the identity of the cell lines. (**C**) Western blots probed for TOP1MT antibody confirm the TOP1MT expression in stably transduced cell lines. VDAC was probed as a load control. (**D**) Quantification of western blots from four replicates shows the fold change in protein abundance compared with VDAC control from four different replicates. All statistical analysis were done using unpaired student *t*-test; where error bars represent standard error of mean and *P*-values ** $< 0.01$, **** $< 0.0001$ and 'ns' signifies no significant differences between indicated groups. Error bars represent standard error of mean. (**E**) Representative confocal images of TOP1MT localization in stable lines where fixed cells were stained for immunofluorescence with anti-TOMM20 (mitochondria, magenta) and anti-TOP1MT (green) primary antibodies. Viral transduction was confirmed by the expression of mCherry (blue). The final column shows the zoom-in of the region indicated by the white dashed box in the merged column. Images confirm the mitochondrial localization of TOP1MT-P193L patient variant. Scale bar represents 10 $\mu$m. Uncropped images of the western blot are available in Supplementary Material, Figure S8b.

consistent with the variant being unable to completely rescue the effects of TOP1MT loss.

## Mitochondrial transcription

We next examined the expression of mtDNA-encoded transcripts, as the supercoiling extent of mtDNA directly influences the transcription of the mitochondrial genome (37–39). Although the WT TOP1MT could restore mitochondrial transcript levels, the P193L variant was slightly less efficient at doing so (Fig. 6A). This reduced rescue is likely because TOP1MT alters mtDNA topology, which impacts mitochondrial transcription *in vitro* (59–63).

## mtDNA copy number and replication

In addition to the effect on transcription, we wanted to determine the ability of the P193L variant to reverse the elevated mtDNA copy number (Fig. 6B) and reduced mtDNA replication rates (Fig. 6C) observed in KO-ctrl cells. In this regard, the P193L variant was able to rescue steady state mtDNA copy number levels to a similar degree as the WT protein. To look at mtDNA replication rates, we monitored the rescue of mtDNA copy number following depletion by ethidium bromide (EtBr). Although the P193L variant showed improved mtDNA repletion compared with the HCT116 KO cells, with nearly complete rescue by day 8,

mtDNA replication was significantly slower than that in cells re-expressing the WT TOP1MT protein, again indicative of reduced functionality.

## Expression of mitochondrial proteins

As TOP1MT can also impact the translation of mitochondrial proteins independently of its topoisomerase activity and changes in transcripts (39), we studied the effect of P193L on the expression of oxidative phosphorylation (OxPhos) proteins encoded by both the nucleus (NDUFB8, SDHB, UQCRC2 and ATP5) and mtDNA (COXII) (Fig. 6D). Notably, global OxPhos protein levels can reflect mitochondrial translation, as the levels of nuclear-encoded OxPhos proteins depend on the expression of mtDNA-encoded subunits (64). Expression of Complex I subunits NDUFB8, Complex II subunit SDHB, Complex III subunit UQCRC2, Complex IV subunit COXII and Complex V subunit ATP5A (Fig. 6E) showed similar trends with reduced expression in P193L cells compared with Rescue. Although we did not see a significant decrease in SDHB and UQCRC2 in these experiments, the results were trending in the same direction. Combined, these results indicate that the P193L variant is unable to completely restore reduced OxPhos proteins expression.
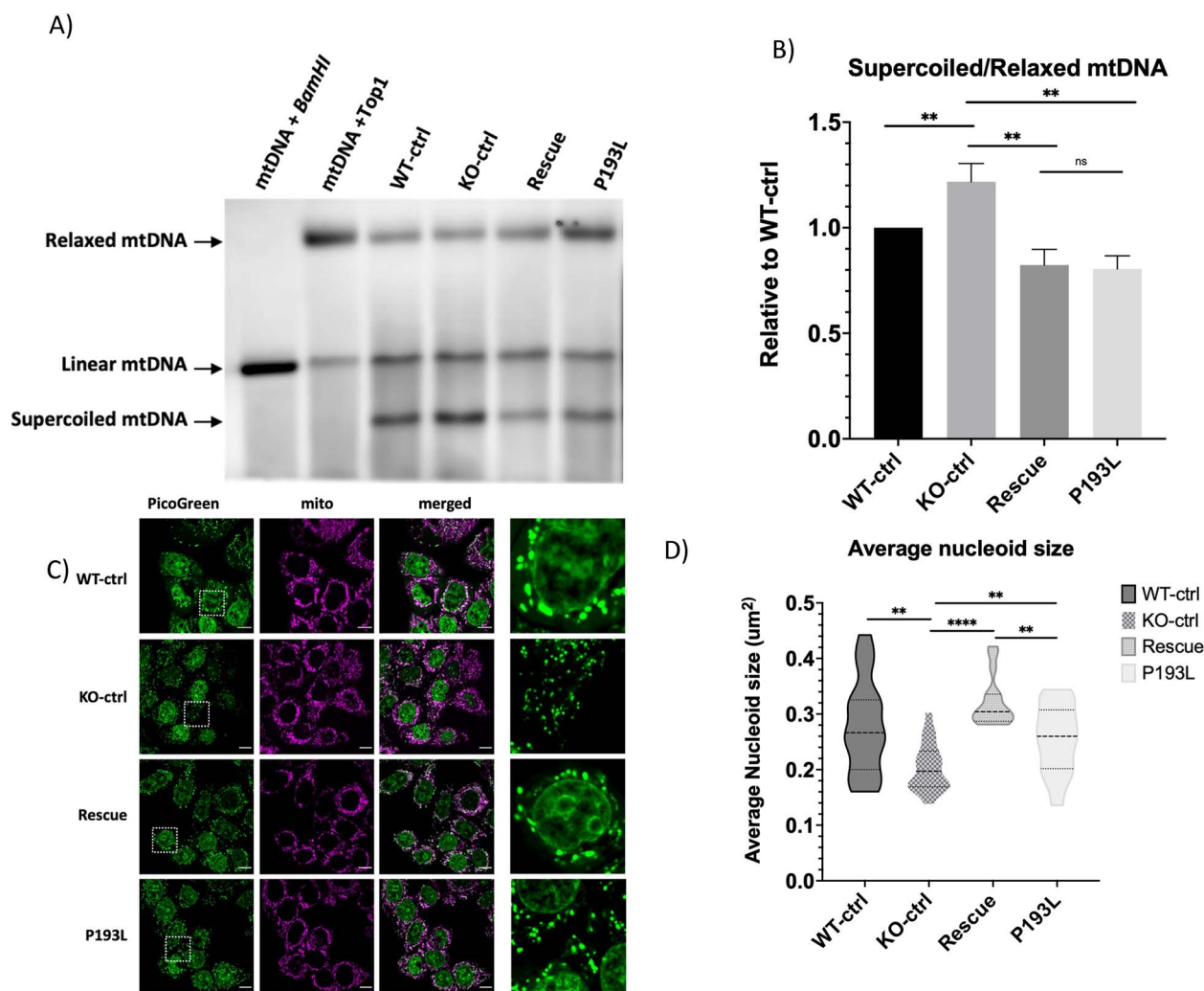
**Figure 5.** TOP1MT-KO cells stably expressing P193L alter mitochondrial genome supercoiling. (**A**) Representative southwestern blot showing increased supercoiled mtDNA in KO ctrl cells and P193L cells. (**B**) Quantification of the ratio of supercoiled to relaxed mtDNA from southwestern blots as in (a) from four independent experiments, normalized relative to control cells. (**C**) Representative confocal images of live cells stained with MitoTracker Far Red (mitochondria) and PicoGreen (dsDNA: nuclear and mtDNA), where the final column shows a zoom-in of the region indicated in the white dashed box for the PicoGreen signal. Scalebars represent 10 $\mu$m. (**D**) Violin plots showing quantification of the average mtDNA nucleoid sizes from 25 cells stained as in (c). All statistical analysis were done using unpaired student $t$-test and P-values **quantification of the average mtDNA nucleoid < 0.01, **** < 0.0001 and 'ns' signifies no significant quantification of the average mtDNA nucleoid differences between indicated groups. Error bars quantification of the average mtDNA nucleoid represent standard error of mean.

## Mitochondrial respiration

Following up on the changes in OxPhos proteins, we next investigated mitochondrial respiration in our stable cell lines (Fig. 6F) to examine if the reduced expression of OxPhos proteins affect the oxygen consumption and mitochondrial energy production. As seen previously (39,65), we found that basal respiration (Fig. 6G), maximal respiration (Fig. 6H) and ATP-coupled respiration (Fig. 6I), were all reduced in the KO-ctrl cells, and restored by re-expressing the WT TOP1MT protein. However, the cells re-expressing the P193L patient variant showed no rescue at all relative to the KO-ctrl cells. Notably, this finding is consistent with patient-derived white blood cells showing impaired OxPhos (Supplementary Material, Fig. S2).

## cGAS-STING pathway in rescue cell lines

Finally, we examined the effect of the P193L variant on the novel cGAS-STING pathway activation that we described earlier in the HCT116 KO cells. For this purpose, we started by looking at the cytosolic mtDNA levels. Unexpectedly, both lines stably

overexpressing either WT or P193L forms of TOP1MT rescued the cytosolic mtDNA levels to the same extent (Supplementary Material, Figs S5a–c). Similarly, qRT-PCR analysis of type I interferon expression was rescued in HCT116 KO cells overexpressing either WT or P193L forms of TOP1MT (Supplementary Material, Fig. S5d). Meanwhile, high level expression of other TOP1MT variants linked to cardiomyopathy (Supplementary Material, Figs S5a and b), namely R198C and V338L, also rescued the cytosolic mtDNA (Supplementary Material, Fig. S5c) and the interferon levels (Supplementary Material, Fig. S5d). However, these lines express TOP1MT protein at ∼10-fold above endogenous levels, which we reasoned could be compensating for a loss of activity in the P193L protein.

## Characterization of low re-expression of P193L and WT TOP1MT variants

To avoid the complications of high level TOP1MT protein expression, we used flow cytometry to sort for cells expressing relatively low levels of mCherry, which should correlate directly
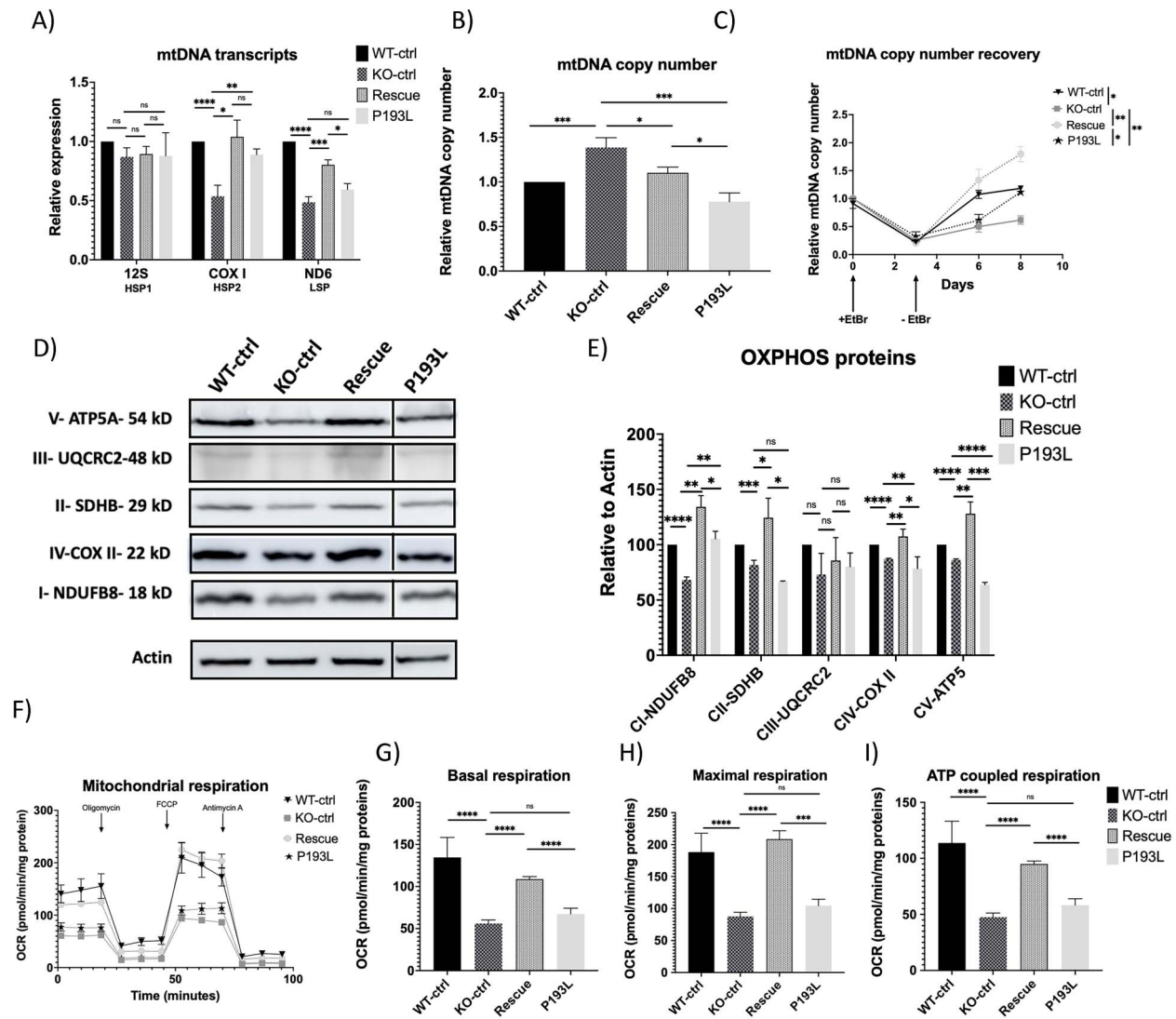
**Figure 6.** TOP1MT-KO cells stably expressing P193L affect mitochondrial DNA maintenance. (**A**) Quantification of mtDNA transcripts from three independent biological replicates in the indicated stable cell lines via qRT-PCR for the indicated genes from the three mtDNA promoters [HSP1 (12S), HSP2 (COX I) and LSP (ND6)]. (**B**) Relative mtDNA copy number from three independent biological replicates, determined by qPCR relative to 18S, is rescued in P193L cells. (**C**) Time course of mtDNA copy number changes (via qPCR) of EtBr depletion (3 days, 1 $\mu$g/ml) followed by repletion (5 days, no EtBr), shows slower recovery in P193L cells compared with Rescue cells. Experiment was performed with three biological replicates. (**D**) Representative western blots show reduced levels of the indicated OXPHOS complex proteins in P193L cells. Blots are cropped at the indicated sizes, with full uncropped blots available in Supplementary Material, Figure S8c. (**E**) Quantification of western blots for OXPHOS proteins as in (d), from three independent experiments, corrected to Actin as a load control. Reduction in OXPHOS proteins encoded by both nuclear (i.e. NDUFB8, SDHB, UQCRC2, ATP5) and mtDNA (i.e. COXII) genomes was observed in P193L cells lines. (**F**) Oxygen consumption rates (OCR) analyzed in the indicated cell lines using the Seahorse XF24 extracellular flux analyzer. The OCR data were used to calculate basal respiration (**G**), maximal respiration (**H**) and ATP production (**I**). Data presented is from a representative experiment with five technical replicates. All statistical analysis were done using unpaired student *t*-test and *P*-values * < 0.05, ** < 0.01, *** < 0.001 and **** < 0.0001. 'ns' signifies no significant differences between indicated groups. Error bars represent standard error of mean.

to TOP1MT protein expression. As shown by western blot (Fig. 7A), we were able to select a population of cells expressing TOP1MT protein much closer to endogenous levels (Fig. 7B). These lines were labeled 'Rescue low' and 'P193L low'. We first looked at nucleoid size as a proxy for mtDNA supercoiling, as this assay is more sensitive than the southwestern assay (39). We found that low expression of the P193L variant was unable to rescue nucleoid size to any degree (Figs 7C and D), compared with the partial rescue when the P193L variant was expressed at a high level (Fig. 5D).

Next, we analyzed the cytosolic mtDNA levels from these cells. Although the low-level expression of TOP1MT WT was still able to rescue the cytosolic mtDNA levels, the low-level expression of the P193L variant was unable to provide rescue (Fig. 7E). In a similar fashion, the type I interferon levels remained elevated in cells expressing low levels of the P193L variant but were restored to normal in cells expressing low levels of the WT protein (Fig. 7F). However, low-level expression of R198C and V338L TOP1MT variants linked to cardiomyopathy (39) (Supplementary Material, Figs S6a and b), fully rescued the nucleoid size (Supplementary Material, Fig. S6c), the cytosolic mtDNA (Supplementary Material, Fig. S6d) and the interferon levels (Supplementary Material, Fig. S6e), suggesting that the cGAS-STING activation is specific to the P193L variant and pathogenic autoimmune activation. Notably, low expression of P193L also failed to show any rescue of mitochondrial morphology,
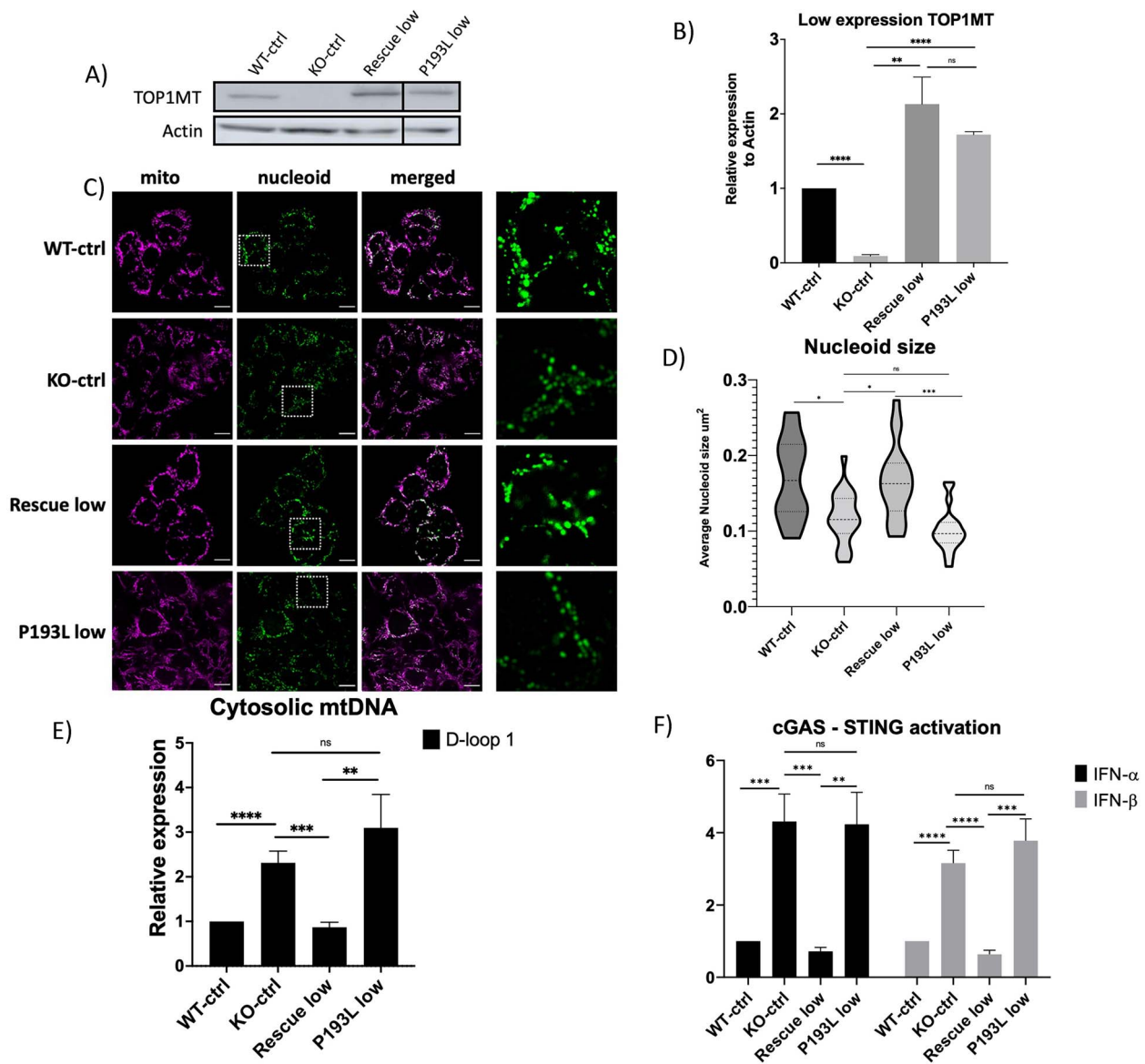
**Figure 7.** TOP1MT-KO cells stably expressing low levels of P193L do not rescue cytosolic mtDNA levels, quantification of the average mtDNA nucleoid reduced nucleoid sizes, or elevated interferon transcripts. (**A**) Representative western blots show near endogenous expression of the TOP1MT protein in cells sorted for lower expression of both WT and P193Lquantification of the average mtDNA nucleoid variants. (**B**) Quantification of western blots of TOP1MT protein as in (**C**), from three independent quantification of the average mtDNA nucleoid experiments, corrected to Actin as a load control. (c) Representative confocal images of live cells stained with MitoTracker Far Red (mitochondria) and PicoGreen (dsDNA: nuclear and mtDNA) where the final column quantification of the average mtDNA nucleoid shows the zoom-in of the region indicated in the white dashed box for the PicoGreen signal. Scale bars represent 10 $\mu$m. (**D**) Violin plots showing quantification of the average mtDNA nucleoid size from 25 cells stained as in (c). (**E**) Quantification of cytosolic mtDNA levels from cells as in (a) via qPCR using the indicated primer set. Normalization was done relative to the corresponding amplicons in total DNA from the same cells. (**F**) qRT-PCR analysis of type I interferon expression from cells as in (a) show elevated type I interferon levels in cells expressing endogenous levels of the P193L variant. All statistical analysis were done using unpaired student $t$-test and P-values * $< 0.05$, ** $< 0.01$, *** $< 0.001$ and **** $< 0.0001$. 'ns' signifies no significant differences between indicated groups. Error bars represent standard error of mean. Uncropped images of western blots are available in Supplementary Material, Figure S8d.

whereas low expression of R198C and V338L showed partial rescue (Supplementary Material, Figs S4c and d).

As another means to examine activation of the cGAS-STING pathway, we used immunofluorescence to monitor the cellular localization of STING, as previous reports show that activated STING translocates from the ER to the Golgi (66). Notably, there is a stronger co-localization signal between STING and the ER in both WT-ctrl and Rescue low lines, compared with the KO-ctrl and P193L low lines (Figs 8A and B). Conversely, there were higher levels of co-localization between STING and Golgi in the

KO-ctrl and P193L low cells, compared with WT-ctrl and Rescue low cell line (Figs 8C and D). These findings are consistent with the P193L variant being unable to rescue cGAS-STING signaling in absence of TOP1MT. Meanwhile, both R198C low and V338L low variants showed a localization pattern similar to the rescue line (Supplementary Material, Figs S8a and b). Altogether, our data provide support for the notion that the P193L variant has impaired functionality, which leads to activation of the cGAS-STING innate immune pathway via promoting the cytosolic release of mtDNA.
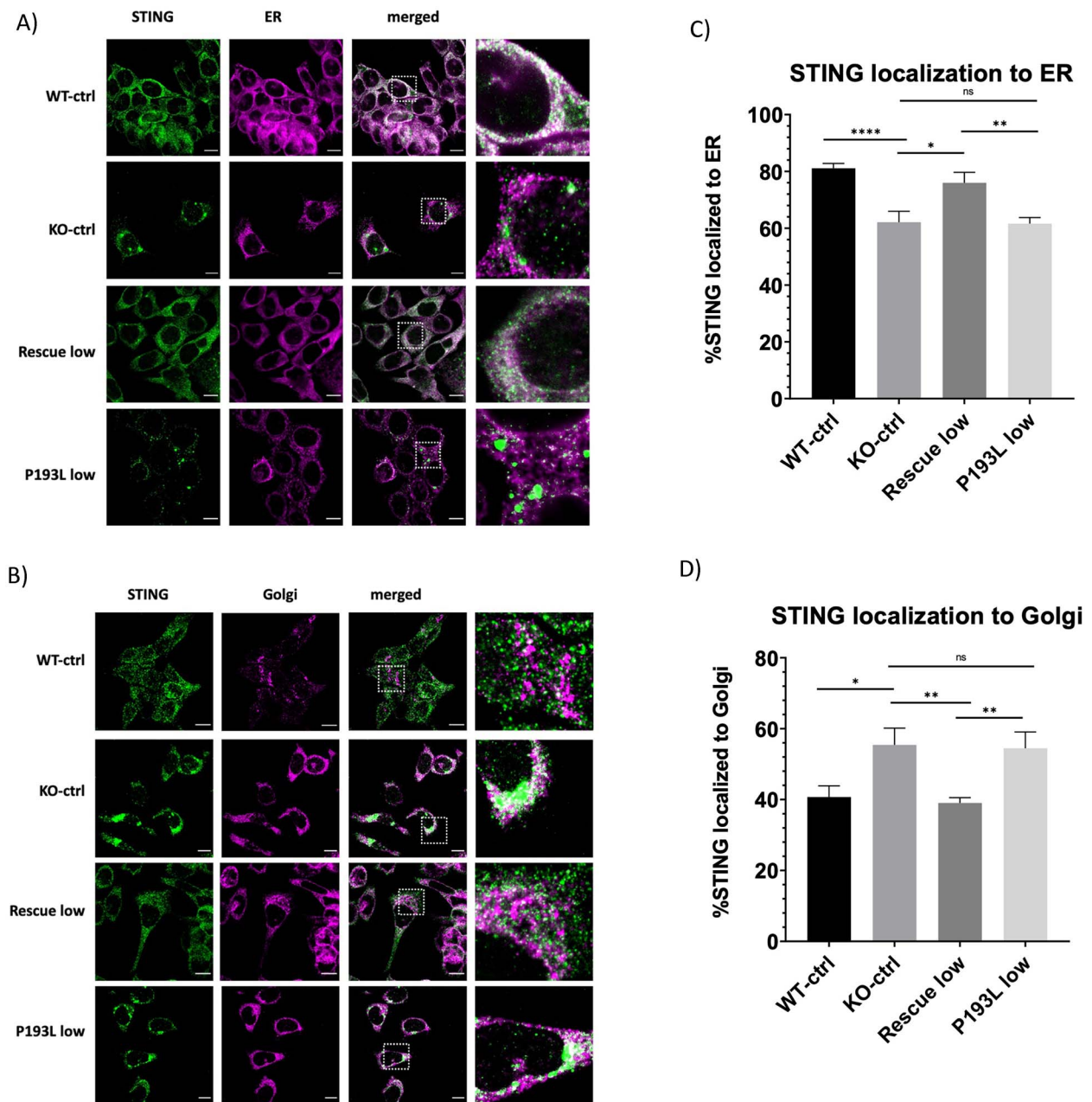
**Figure 8.** STING relocates from the ER to the Golgi in TOP1MT KO and P193L low cells. Representative confocal images of fixed cells to visualize the co-localization (white) of STING (green) with either the ER or Golgi (magenta). (**A**) Cells stained with primary antibodies for immunofluorescence with anti-STING (green) and anti-Calnexin (ER, magenta. (**B**) Cells stained with primary antibodies for immunofluorescence with anti-STING (green) or anti-TGN46 (Golgi, magenta). The final column shows the zoom-in of the region indicated by the white dashed box in the merged column. Scale bar represents 10 $\mu$m. Localization of STING to the Golgi, and the absence of STING in the ER, which are indicative of STING activation, were observed in the TOP1MT KO and P193L low lines and confirmed by quantification of the percentage of STING signal co-localizing to the ER (**C**) or Golgi (**D**) from at least 10 images as in (a) and (b), respectively. All statistical analysis were done using unpaired student t-test and P-values* < 0.05, ** < 0.01 and **** < 0.0001. 'ns' signifies no significant differences between indicated groups. Error bars represent standard error of mean.

## Discussion

The discovery of the novel TOP1MT missense P193L variant present among multiple family members with autoimmune phenotypes led us to investigate whether TOP1MT could impact mtDNA-mediated activation of the cGAS-STING innate immune response. We found that the loss of TOP1MT in HCT116 cells led to increased levels of cytosolic mtDNA and activation of the cGAS-STING pathway, as reflected by increased levels of type I interferons. Demonstrating that this pathway is conserved in

multiple cell types and organisms, we found that depletion of TOP1MT in both human fibroblasts and MEFs also resulted in activation of cGAS-STING signaling. To show that the interferon signaling is dependent on the cGAS-STING pathway, we found that the cGAS inhibitor RU.521 blunts signaling in HCT116 *TOP1MT* KO cells, whereas genetic ablation of cGAS also prevented the signaling in MEFs depleted of TOP1MT.

Having established a novel link between TOP1MT loss of function and mtDNA-mediated cGAS-STING activation, we also

investigated the impact of three TOP1MT variants on this pathway. We found that when expressed close to endogenous levels, the P193L variant was unique among the three TOP1MT variants we interrogated in its inability to rescue the mtDNA release and cGAS-STING activation phenotype. This finding supports the idea that the P193L variant may contribute to the autoimmune phenotypes in our family of interest, as the other variants, which are not linked to autoimmune phenotypes, were able to rescue the cGAS-STING activation. This finding also highlights the fact that rare variant burden testing for correlation of genotypes to phenotypes in TOP1MT must be supported by functional studies, as variants that do not exhibit the relevant functional properties will dilute the signal that is conferred by variants that do impact disease relevant functions.

Our findings show that the P193L variant is not fully functional. In addition to the inability of low levels of the P193L variant to reverse cGAS-STING activation in cells lacking TOP1MT, we found that it was unable to rescue several other mitochondrial phenotypes linked to TOP1MT function, even when expressed at high levels (summarized in Table 3). Importantly, the fact that the P193L variant was overexpressed by ~10-fold in our cellular model system, likely means that we are overestimating the partial functionality of this variant. Nonetheless, high expression of the P193L variant was only capable of partially rescuing nucleoid size, transcript levels and mtDNA copy number recovery. Similarly, mitochondrial morphology was also only partially rescued by expression of the P193L variant. Although the mechanistic connection between TOP1MT and mitochondrial morphology remains unknown, it is tempting to speculate that this likely also involves the role of TOP1MT in regulating mtDNA. Meanwhile, the P193L variant was unable to restore steady state levels of OxPhos proteins, as well as several parameters of mitochondrial respiration. This finding suggests that the role of TOP1MT in mitochondrial translation, which is distinct from its topoisomerase activity, likely contributes to the reported mitochondrial dysfunction in patient blood cells. The finding that translation is more severely impaired than topoisomerase activity for the P193L variant is similar to previous work for two other TOP1MT variants, R198C and V338L (39).

Intriguingly, the correlation between lack of topoisomerase activity, mtDNA release and elevated cGAS-STING signaling suggests that the topoisomerase activity of TOP1MT is required to prevent mtDNA release, rather than the other characterized functions of TOP1MT in transcription or translation. In this context, it is notable that R198C and V338L TOP1MT variants have impaired transcription or translation activities, but retain greater topoisomerase activity, and are able to rescue mtDNA release and cGAS-STING activation. These observations further support the notion that the transcription and translation functions of TOP1MT are not involved in mtDNA release. Nonetheless, we cannot exclude the possibility that some other, perhaps unrecognized, function of TOP1MT plays a role in preventing mtDNA release into the cytosol. Moreover, exactly how the P193L variant mechanistically leads to cytosolic release of mtDNA remains unknown. Another unresolved question is how does the P193L variant impact protein activity. In this regard, it may be notable that the P193L variant is located within the core barrel of TOP1MT, which is predicted to bind nucleic acids.

Although *TOP1MT* is not yet formally annotated to the clinome as a disease gene, increasing evidence suggests that some functional *TOP1MT* variants may indeed be pathogenic (39,67). For example, an *in vitro* study showed that some TOP1MT variants have reduced DNA relaxation activities, including E168G, which

has been described in a patient with mitochondrial deficiency syndrome (68). Meanwhile, two other TOP1MT variants were identified in a patient with a pediatric cardiomyopathy (39). The fact that the P193L variant we describe here was identified within an extended pedigree that had multiple members affected with SLE and other autoimmune diseases suggests that this is a novel pathogenic phenotype linked to TOP1MT dysfunction. However, it is not possible to rule out polygenic contributions from other genes, as no comprehensively diagnostic 'lupus panel' exists to this end. To date, there are only a limited number of reports of potential pathogenic TOP1MT variants, which are associated with diverse pathogenic phenotypes (39,67–69). As such, more examples with shared phenotypes need to be identified before TOP1MT can officially be definitively considered as a disease gene. Nonetheless, future studies looking to establish the genetic cause of SLE should also consider variants in TOP1MT. Similarly, variants in other genes encoding proteins linked to mtDNA release (e.g. TFAM, POLG, CLPP, ATAD3B) could also be considered in autoimmune diseases (23,24,70,71).

Genetic, epigenetic or environmental risk factors have been implicated as underlying causes of SLE (72); however, the underlying mechanism behind the disease is not always clear. With respect to whether the P193L variant contributes to the SLE phenotype in the proband and her family members affected with lupus and other autoimmune diseases, it is important to consider the already-established links between SLE and mitochondrial dysfunction. For example, general mitochondrial dysfunction and aberrant oxygen metabolism have a role in many autoimmune diseases, including SLE (73–75). Meanwhile, links between SLE and the cGAS-STING innate immune response are also important in the context of considering the contribution of TOP1MT dysfunction to SLE. Consistent with the notion the cGAS-STING activation contributes to SLE, previous reports have noted cGAS-STING activation in a subset of SLE cases (76,77). Some of this previous work implicated nuclear DNA as the cytosolic dsDNA trigger, as studies identified impaired function of the nuclear DNA repair machinery can lead to SLE (78–84). However, it is worth noting that much of the mitochondrial DNA repair machinery is shared with the nuclear repair machinery. Thus, it is likely that the impairments in nuclear DNA repair enzymes that are linked to SLE also impact mtDNA. The fact that some SLE patients exhibited increased levels of mtDNA damage (85) supports this notion and argues that mtDNA damage may contribute to SLE. Moreover, it is notable that topoisomerases, including TOP1MT, can participate in DNA repair (86,87). Collectively, this previous work linking SLE, mitochondrial dysfunction and the cGAS-STING pathway, support the argument that the P193L variant in TOP1MT could contribute to SLE.

Another intriguing connection between SLE and TOP1MT is that fact that autoantibodies recognizing the nuclear topoisomerase enzyme TOP1 have been described in patients with SLE (44–47). Notably, these TOP1 autoantibodies recognize the highly conserved catalytic domain of TOP1 (88), which is conserved with TOP1MT. Given the novel connection that we describe here between TOP1MT and SLE, it is tempting to speculate that these autoantibodies are in fact made against TOP1MT and cross-react with TOP1, even though they were first shown to bind TOP1. This notion is supported by the fact that SLE sera recognize TOP1MT (89). Given that 19% of autoantibodies collected from patients with SLE were able to detect TOP1MT (48), it is possible that TOP1MT plays a much wider role in SLE than currently appreciated. For example, if TOP1MT released from mitochondria along with mtDNA, these autoantibodies could also contribute to

an elevated immune response contributing to SLE. Thus, beyond our current study, there is considerable evidence supporting the argument that TOP1MT plays a role in SLE.

The novel connection we describe here between TOP1MT, cGAS-STING and SLE has important clinical implications, as identifying novel SLE candidate genes such as TOP1MT, and understanding the mechanistic underpinnings of mtDNA-mediated inflammation, will be important for personalized medicine approaches. As we learn more about the different causes of SLE and their underlying mechanisms, this will provide a clearer picture of which treatments might be beneficial. For example, cGAS inhibitors like RU.521 may prove to be effective in patients where the cGAS-STING pathway is elevated. Meanwhile, it is also important to consider the effects of drugs that impact mtDNA, a key example being the chemotherapeutic agent doxorubicin, which causes mtDNA damage, cytosolic release of mtDNA and activation of the cGAS-STING pathway (68,90,91). Although cGAS-STING activation by doxorubicin may be advantageous by activating innate immune signaling in cancer (92), it could be detrimental in other circumstances by activating the immune response inappropriately. In this regard, loss of TOP1MT increases sensitivity to doxorubicin treatment (76), suggesting TOP1MT variants could be relevant to the inflammatory cardiotoxicity associated with this commonly used cancer drug.

## Conclusions

In summary, this report provides the first evidence linking TOP1MT to release of mtDNA to the cytosol, activation of the innate immune response through the cGAS-STING pathway, and ultimately increased levels of interferons. Our findings also support the notion that the P193L variant could contribute to the autoimmune phenotypes in the patients, and provide novel mechanistic insight how mitochondrial dysfunction might contribute to autoimmune diseases via mtDNA-mediated activation of innate immunity. A better understanding of the causes of autoimmune diseases will help to elucidate the complex heterogeneity of these diseases, and could lead to novel therapeutic approaches.

## Materials and Methods
### Mutation identification

In accordance with the principles of the Declaration of Helsinki, all study participants provided informed consent to next-generation sequencing as part of the BCCHRI study 'Comprehensive Characterization of Genetic Disorders of Body Weight' (UBC CREB Study approval number H08–00784).

### Cell culture

Primary MEFs were generated from E12.5–14.5 embryos. Cells were maintained in DMEM (D5756, Sigma-Aldrich) with 10% fetal bovine serum (FBS) (97068–085, VWR). McCoy's 5A (modified) media (Gibco, 16 600–82) containing l-Glutamine and supplemented with 10% FBS was used to culture HCT116 control (HCT116 WT), HCT116 TOP1MT-KO (HCT116 KO) and stably transfected cells. Cells were seeded at $1.5 \times 10^6$ cells seeding density in 10 cm plates and allowed to grow for two days before being harvested for analysis. DMEM (Gibco, 11 965 092) supplemented with 10% FBS was used for Phoenix cells for the retrovirus generation, MEFs and HFF-1 cells. All cells were maintained at 37°C and 5% $CO_2$.

### Plasmids & cloning

The retroviral vector pRV100G backbone was used to insert TOP1MT open reading frame (ORF) followed by C-terminal T2A mCherry tag. Site directed mutagenesis was used to introduce the C578T variant in TOP1MT. The empty vector control was missing the TOP1MT ORF and only contained the backbone with T2A mCherry.

### Generation of stable lines

Stable cells expressing wild-type TOP1MT (NM_052963.2), TOP1MT P193L variant, or empty vector controls were generated via retroviral transduction. Briefly, Phoenix cells were transfected with the retroviral plasmids. Then the HCT116 WT or HCT116 KO cells were transduced using 5 ml of the supernatant containing virus after 48 and 72 h in 100 mm plates. Following transduction, Flow cytometry sorting was done for the red fluorescence from $\sim 6 \times 10^6$ cells were using a 130 $\mu$m nozzle on a BD FACSAria Fusion (FACSAriaIII) cytometer (BD Biosciences), supported by FACSDiva Version 8.0.1. As for the cells with low expression of TOP1MT, all the positively expressing red fluorescent cells were subjected to sorting again separating them into low threshold, intermediate and high expression red fluorescence gates.

### PCR and sequencing

PureLink Genomic DNA Mini Kit (Thermo Fisher Scientific, K182001) was used for total DNA extraction. TOP1MT cDNA was amplified by PCR using the forward primer CACAACAAAG-GAGGTTTTCCGGAAG and the reverse primer TGCAGTCCTTC-CCCAGGA to confirm the success of the transduction. The amplified band was further purified and sequenced using Sanger sequencing to confirm the variant status of TOP1MT.

### Live cell imaging

Live cell imaging was done on 35 mm glass bottom dishes, $8 \times 10^4$ cells were seeded and grown for 2 days. MitoTracker Red (50 nM) (Thermo Fisher Scientific, M7512) and PicoGreen (Thermo Fisher Scientific, P7581) (3 $\mu$l/ml) were used to visualize mitochondrial networks and mtDNA nucleoids, respectively (39,93).

### Immunofluorescence staining

A total of $1.5 \times 10^4$ cells were seeded over 12 mm glass coverslips (no. 1.5) in 24 wells plates and incubated for 2 days. Subsequently, cells were fixed with 4% paraformaldehyde and stained with mitochondrial networks labeled with a primary antibody against TOMM20 (Sigma-Aldrich, HPA011562) used at 1:1000, STING (D2P2F) (Cell signaling, 13647S) used at 1:300, endoplasmic reticulum ER Calnexin (Millipore Sigma, MAB3126) at 1:1000 and Golgi TGN46 (Proteintech, 66 477–1-Ig) used at 1:500. The corresponding Alexa fluor-conjugated secondary antibodies (Thermo Fisher Scientific) were used at 1:1000.

### Fluorescence in situ hybridization

Cells grown on fibronectin-coated coverslips (Fisher Scientific #12–545-81) were fixed at 37°C using a solution of 4% paraformaldehyde in PHEM buffer (60 mM PIPES, 25 mM HEPES, 10 mM EGTA, 4 mM $MgSO_4$, pH 6.8) for 15 min, and then permeabilized with 0.1% (v/v) Triton X-100 in phosphate buffered saline (PBS) for 10 min at room temperature. FISH was then performed as previously described (94,95), using the mREP probe conjugated to Atto633, which was purchased from Integrated DNA Technologies. For immunofluorescence, coverslips were blocked with filtered PBS containing 1% (w/v) BSA at room temperature

for at least an hour, following either permeabilization or FISH. Incubation with primary antibodies was carried out in PBS containing 1% (w/v) BSA at 4°C overnight, followed by 4 × 5 min washes in PBS. Secondary antibodies were incubated in PBS containing 1% BSA for 1 h at room temperature. Secondary antibody was removed by 4 × 5 min washes in PBS. Coverslips were then mounted onto slides using Prolong Glass. The following antibodies were obtained commercially and used at the indicated dilutions for immunofluorescence: cGAS (CST #15102, 1:100), HSP60 (EnCor Biotechnology #CPCA-HSP60, 1:500), DNA (Millipore Sigma #CBL186, 1:200). Secondary antibodies conjugated to Alexa 405, 488 or 647 were purchased from Thermo Fisher and used at 1:500, with the exception of anti-chicken Alexa 405, which was from Abcam and used at 1:250.

## Microscopy

An Olympus spinning disk confocal system (Olympus SD OSR) (UAPON 100XOTIRF/1.49 oil objective) was used to image fixed samples and the microscope was operated by Metamorph software. Whenever there was live imaging, a cellVivo incubation module was used to maintain cells at 37°C and 5% $CO_2$. For FISH and nucleoid-cGAS overlap images, imaging was performed using a Plan-Apochromat ×63/1.4 NA oil objective on an inverted Zeiss spinning disk microscope using 405, 488, 561 and 633 nm laser lines.

## Image analysis for mtDNA nucleoids

The particle analysis tool in ImageJ FIJI was used to measure nucleoid size after binarizing the images (96). A region of interest in cells stained with PicoGreen was manually selected including all the mitochondrial network of the cell but excluding the nucleus, then the surface area of each nucleoid was automatically determined using the analyze particles feature. The nucleoids from at least 10 cells were measured. Data were represented by a violin plot representing the distribution of the average mtDNA nucleoid sizes per cell for the indicated cell lines. *P*-values were on the basis of unpaired, two-tailed Student's *t*-tests.

## Image analysis for mitochondrial networks

Images of the cells stained with anti-Tomm20 (Sigma-Aldrich, HPA011562) were used for qualitative evaluation of the mitochondrial network morphology. The network was classified into three categories, fragmented (predominantly small mitochondrial fragments), intermediate (cells containing a mixture of short fragments and elongated networks) and fused (elongated, interconnected networks with few to no short fragments) (93). At least 50 cells from three independent biological replicates were scored for each of the investigated cell lines. The results shown represent means ± SEM, and *P*-values were on the basis of unpaired, two-tailed Student's *t*-tests.

## Image analysis for STING localization

Images of the cells stained with anti-STING (D2P2F) (Cell signaling, 13647S), anti-Calnexin (Millipore Sigma, MAB3126) and anti-TGN46 (Proteintech, 66 477–1-Ig) were used for quantitative evaluation of the localization of STING to either the ER or the Golgi. Images were binarized, then the surface area of the total STING signal or the localized signal to the corresponding organelle were measured. The ratio of the localized area to the total STING area was determined from at least 10 images. Data were represented as means ± SEM, and *P*-values were on the basis of unpaired, two-tailed Student's *t*-tests.

## Image analysis of cytoplasmic nucleoids and overlap with cGAS

The mitochondria channel was masked using automatic thresholding, and this mask was subtracted from the mtDNA FISH channel using the image calculator in Fiji. Any remaining mtDNA FISH signal that did not overlap with anti-DNA immunofluorescent puncta were subtracted from analysis. The number of remaining mtDNA FISH puncta, as well as their overlap with cGAS, was scored.

## mtDNA copy number analysis

The PureLink Genomic DNA Mini Kit (Thermo Fisher Scientific, K182001) was used to isolate total DNA from cultured cells using according to the manufacturer's protocol. Quantitative PCR (QPCR) was used to determine mtDNA copy number (97). Primers shown in Table 1 for mtDNA or 18S DNA were used with PowerUp SYBR Green Master Mix (Thermo Fisher Scientific, A25742) to amplify 50–100 ng of DNA template, in the QuantStudio 6 Flex Real-Time PCR system (Thermo Fisher Scientific) machine. The delta delta Ct method was used to determine mtDNA copy number using the 18S gene as a reference. Reactions were performed in three technical replicates and mtDNA copy number analysis was performed on at least three independent biological replicates. Data are presented as mean ± SEM and unpaired, 2-tailed Student's *t*-tests were used to determine statistical significance.

## EtBr depletion/repletion

In total, 1 $\mu$g/ml EtBr (Fisher Scientific, 15–585-011) was used to deplete the cells from their mtDNA content for three days, as described previously (54), then fresh media was added afterwards to allow the cells to recover their mtDNA copy number. Cell pellets from days 0, 3, 6 and 8 were collected for DNA purification and copy number analysis.

## Western blot

RIPA buffer (Thermo Scientific™, 89 900) containing protease inhibitors was used to lyse collected cell pellets after washing with 1× PBS. SDS-PAGE gels were used to resolve 50 $\mu$g of total cell lysates from different cell lines then polyvinylidene fluoride (PVDF) membranes were used for the transferred blot. Blots were probed with several antibodies at the indicated dilutions; OxPhos antibody cocktail (Abcam, ab110411; 1:500 dilution), anti-Actin (Sigma, A5316; 1:1000), anti-MTCO2 (Abcam, ab110258; 1:1000), anti-GAPDH (Millipore Sigma, ABS16; 1:1000), anti-TOP1MT-3 (Developmental Studies Hybridoma Bank, CPTC-TOP1MT-3; 1:200). Appropriate horseradish peroxidase (HRP)-conjugated secondary antibodies were used at 1:3000 as follows: goat anti rabbit IgG, HRP linked Antibody (Cell Signaling Technology, 7074S) or goat anti-mouse IgG-HRP (Santa Cruz Biotechnology, sc-2055). The Clarity ECL substrate (Biorad, 1 705 061) was used to expose the horseradish enzyme attached to each antibody using an Amersham Imager AI600.

## Southwestern blot

Cells were treated with 10 uм Aphidicolin (HelloBio Ltd, Bristol UK) for 4 h to inhibit nuclear DNA synthesis, then 50 uм BrdU (Invitrogen, fisher scientific) is added for another 24 h. Total DNA was isolated from $2 × 10^7$ cells according to the instruction of E.Z.N.A Tissue DNA kit. As controls, 1ug of DNA was treated with 10 U of Topoisomerase I (New England Biolabs) at 37°C for 1 h, or BamHI 20 U (New England Biolabs) at 37°C for 1 h. DNA samples (1 ug)

**Table 1.** Primers used for quantitative PCR for detection of indicated genes

| Gene | Forward Primer | Reverse Primer |
|---|---|---|
| 18 S | TAGAGGGACAAGTGGCGTTC | CGCTGAGCCAGTCAGTGT |
| mito | CACCCAAGAACAGGGTTTGT | TGGCCATGGGTATGTTGTTAA |
| COX I | GACGTAGACACACGAGCATATTTCA | AGGACATAGTGGAAGTGAGCTACAAC |
| ND 6 | CAAACAATGTTCAACCAGTAACCACTAC | ATATACTACAGCGATGGCTATTGAGGA |
| Cyt B | ATCACTCGAGACGTAAATTATGGCT | TGAACTAGGTCTGTCCCAATGTATG |
| Actin | AAGACCTGTACGCCAACACA | AGTACTTGCGCTCAGGAGGA |
| IFN-$\alpha$ | AAATACAGCCCTTGTGCCTGG | GGTGAGCTGGCATACGAATCA |
| IFN-$\beta$ | AAGGCCAAGGAGTACAGTC | ATCTTCAGTTTCGGAGGTAA |
| IFN-$\gamma$ | CGCCTTGGAAGAGTCACTCA | GAAGCCTCAGGTCCCAATTC |
| STING | GAGCAGGCCAAACTCTTCTG | TGCCCACAGTAACCTCTTCC |
| D-loop 1 | TTTCCCCTCCCACTCCCATA | GTGTGTGTGCTGGGTAGGAT |
| D-loop 2 | CACCCAAGAACAGGGTTTGT | TGGCCATGGGTATGTTGTTAA |
| mTop1mt | AGTCTTAGCTTACAACCGGGC | GTGTCTGCATCGACTTCTCG |
| mCxcl10 | CCAAGTGCTGCCGTCATTTTC | GGCTCGCAGGGATGATTTCAA |
| mIfit1 | CAAGGCAGGTTTCTGAGGAG | GACCTGGTCACCATCAGCAT |
| mIfit3 | TTCCCAGCAGCACAGAAAC | AAATTCCAGGTGAAATGGCA |
| mIfnb1 | CCCTATGGAGATGACGGAGA | CCCAGTGCTGGAGAAATTGT |
| hTOP1MT | GGGATGGCAAGTCCAGG | CTTGTTCTCCTCCTTGTCCG |
| hCXCL10 | CACCATGAATCAAACTGCGA | GCTGATGCAGGTACAGCGT |
| hIFIT1 | GCAGCCAAGTTTTACCGAAG | GCCCTATCTGGTGATGCAGT |
| hIFI44L | CAATTTAAGCCTGATCTAACCCC | CAGTTGCGCAGATGATTTTC |

were then separated on a 0.45% agarose gel (Biotechnology VWR, life science) at 30 V 18–20 h in cold room. The gel was washed briefly with water and soaked in denaturing buffer (0.5 N NaOH, 1.5 M NaCl) for 45–60 mins. The gel was washed again in water and soaked in 10× saline-sodium citrate (SSC) for 30 mins. Transfer to PVDF membrane (Bio-Rad, Cat# 1620177) was done using capillary action as described previously (Nature protocols, 518, 2006). The PVDF membrane was washed in 6× SSC for 2 min, and the DNA bands on the membrane were immobilized by ultraviolet-crosslinking (UV Stratalinker 1800). After blocking with 10% non-fat dry milk for 1 h, the PVDF membrane was incubated for 2 h at 20°C with anti-BrdU antibody (1:2000× dilution in TBST, Becton Dickinson Immunocytometry Systems), followed by incubations with corresponding HRP-conjugated goat polyclonal anti-mouse IgG (1:5000 dilution, EMD Millipore Etobicoke, Ontario, Canada). Blots were developed with Supersignal West Femto enhanced chemiluminescence substrate (Thermo Scientific) and imaged using the chemiluminescence imaging analyzer (LAS3000mini; Fujifilm, Tokyo, Japan).

## RNA extraction and quantification

The E.Z.N.A.® HP Total RNA Kit, Omega Bio-tek® (VWR Scientific, CA101414–850) was used for RNA extraction from cell pellets according to the manufacturer's protocol. Following extraction, 7.5 $\mu$g of RNA was reverse transcribed by iScript™ Advanced cDNA Synthesis Kit (Biorad, 1 725 038) to generate cDNA. Quantitative PCR with PowerUp SYBR Green Master Mix (Thermo Fisher Scientific, A25742) was used to amplify the genes of interest according to the primers mentioned in the Table 1 from 15–20 ng of cDNA in the QuantStudio 6 Flex Real-Time PCR system (Thermo Fisher Scientific) machine. Actin expression was used as the control in the delta delta Ct method to determine the relative expression of various transcripts. Reactions were performed in triplicate and mtDNA copy number analysis was performed on at least three independent biological replicates. Data are presented as mean ± SEM and unpaired, two-tailed Student's *t*-tests were used to determine statistical significance.

## Cytosolic mtDNA quantification

Cell pellet was resuspended in roughly 500 $\mu$L buffer containing 150 mM NaCl, 50 mM HEPES, pH 7.4 and 15–25 $\mu$g/ml digitonin (Sigma Aldrich, D141). The homogenates were incubated end over end for 25 min to allow selective plasma membrane permeabilization, then centrifuged at 980 g for 10 m to pellet intact cells. The first pellet was used to extract total DNA using the PureLink Genomic DNA Mini Kit (Thermo Fisher Scientific, K182001). The cytosolic supernatants were transferred to fresh tubes and spun at 17 000 g for 10 m to pellet any remaining cellular debris, yielding cytosolic preps free of nuclear, mitochondrial and ER contamination. DNA was then isolated from these pure cytosolic fractions using the PureLink Genomic DNA Mini Kit (Thermo Fisher Scientific, K182001). qPCR was performed on both whole cell extracts and cytosolic fractions using nuclear DNA primers (18S) and mtDNA primers (D loop1–2, CytB, COX I, ND 6) as indicated in Table 1, and the CT values obtained for mtDNA abundance for whole cell extracts served as normalization controls for the mtDNA values obtained from the cytosolic fractions. This allowed effective standardization among samples and controlled for any variations in the total amount of mtDNA in control and stable cell lines samples.

## cGAS inhibition and recovery

RU.521 (Invivogen, inh-ru521) was used at a concentration of 5 ug/ml to inhibit cGAS in cells seeded in 10 cm plates, after 24 h fresh media was added to the cells to recover for another 24 h. Similar volume of dimethyl sulfoxide (DMSO) was used as a negative control to eliminate any effect of the drug solvent.

## Structural modeling

Structural models for the TOP1MT variants were generated via RoseTTAFold, a deep learning solution to predicting protein structures, which was conducted on the Robetta web server (98). Five structures were generated per mutant, the structure with the highest confidence level was selected for further use in analysis. Once the structures were selected for each mutant, HADDOCK

**Table 2.** siRNA duplexes sequences used to knockdown TOP1MT in MEF and HFF-1 cells

|  | Sense | antisense |
|---|---|---|
| Mouse siTop1mt | rCrCrUrGrCrArArArGrUrCrUrUrArGrCrUrUrArCrArArCCG | rCrGrGrUrUrGrUrArArGrCrUrArArGrArCrUrUrUrGrCrArGrGrUrU |
| Human siTOP1MT | rCrArGrCrUrArArGrArUrCrUrUrArUrCrCrUrArCrArArCCG | rCrGrGrUrUrGrUrArGrGrArUrArArGrArUrCrUrUrArGrCrUrGrCrU |

**Table 3.** Summary of analyzed phenotypes for high levels of P193L variant. Analyzed phenotypes where +++ represents full rescue, ++ represent moderate rescue, + for weak rescue and – for no rescue at all

|  | KO-ctrl | Rescue | P193L |
|---|---|---|---|
| Nucleoid size | Smaller | +++ | + |
| Supercoiling | Higher | +++ | ++ |
| mtDNA Copy number | Higher | +++ | +++ |
| mtDNA Repletion | Slower | +++ | ++ |
| Mitochondrial Transcripts | Lower | +++ | + |
| OXPHOS Proteins | Lower | +++ | + |
| Mitochondrial Oxygen consumption | Lower | +++ | – |
| Mitochondrial morphology | Fused | +++ | + |
| cGAS-STING activation | Activated | +++ | ++ |

was used to perform docking (99,100). The binding strength and location of the binding were approximated to generate models with both short (10) and long (50) strands of mtDNA, with sequences detailed in the following reference (36, 90). Short strand docking offered insight into the highly charged barrel through the middle of the protein. Long strand modeling then mixed the barrel analysis with the stabilizing forces of the surrounding protein structure. The most probable binding sites were identified and fit by HADDOCK and the model selected was the one with the best HADDOCK score. These models and the interaction lists generated around them were used then to compare the binding efficacy and form between the mutants and the wild-type. Models were downloaded, screened and visualized in Pymol (101).

## TOP1MT knockdown

siRNA transfection was performed with 25 nM siRNA duplexes (Integrated DNA Techonologies), shown in the Tables 2, using 3 uL of Lipofectamine RNAiMAX reagent (ThermoFisher Scientific, 13 778 150) according to the manufacturer's protocol.

## Supplementary Material

Supplementary Material is available at *HMG* online.

## Acknowledgements

## Data Availability

The authors confirm that the data supporting the findings of this work are available within the article and its Supplementary material. Raw data supporting these findings are available from the corresponding author upon reasonable request.

*Conflict of Interest statement.* The authors declare that they have no conflict of interest.

## Funding

## Author Contributions

I.A.K. conceived the study, designed, performed and analyzed experiments and wrote the manuscript. J.D. performed southwestern blot and cytosolic mtDNA experiments. Y.L and S. T.-O. performed the work in mouse and human fibroblast lines. G.R.R. and L.E.N. performed the FISH experiments. B.K.C. performed the experiments on patient-derived lymphoblastoid cell lines. A.S. generated the structural model. H.Z., S.N.H. and Y.P. generated the HCT116 *TOP1MT* KO cells, shared the TOP1MT cDNA, and provided input on the project. A.K. provided input on the project and edited the manuscript. G.S.S. and A.P.W. helped design and supervise the study. W.T.G. identified the family bearing the *TOP1MT* patient variants, including clinical and family history, provided input on the project and edited the manuscript. T.S. conceived and designed the study, analyzed experiments, supervised the study and wrote the manuscript.

# References

1. Wincup, C. and Radziszewska, A. (2021) Abnormal mitochondrial physiology in the pathogenesis of systemic lupus erythematosus. *Rheum. Dis. Clin. N. Am.*, **47**, 427–439.

2. Yang, S.K., Zhang, H.R., Shi, S.P., Zhu, Y.Q., Song, N., Dai, Q., Zhang, W., Gui, M. and Zhang, H. (2020) The role of mitochondria in systemic lupus erythematosus: a glimpse of various Pathogenetic mechanisms. *Curr. Med. Chem.*, **27**, 3346–3361.

3. Alperin, J.M., Ortiz-Fernández, L. and Sawalha, A.H. (2018) Monogenic lupus: a developing paradigm of disease. *Front. Immunol.*, **9**, 2496.

4. Bursztejn, A.C., Briggs, T.A., del Toro Duany, Y., Anderson, B.H., O'Sullivan, J., Williams, S.G., Bodemer, C., Fraitag, S., Gebhard, F., Leheup, B. *et al.* (2015) Unusual cutaneous features associated with a heterozygous gain-of-function mutation in IFIH1: overlap between Aicardi-Goutières and singleton-Merten syndromes. *Br. J. Dermatol.*, **173**, 1505–1513.

5. An, J., Briggs, T.A., Dumax-Vorzet, A., Alarcón-Riquelme, M.E., Belot, A., Beresford, M., Bruce, I.N., Carvalho, C., Chaperot, L., Frostegård, J. *et al.* (2017) Tartrate-resistant acid phosphatase deficiency in the predisposition to systemic lupus erythematosus. *Arthritis Rheumatol*, **69**, 131–142.

6. Crow, Y.J., Chase, D.S., Lowenstein Schmidt, J., Szynkiewicz, M., Forte, G.M., Gornall, H.L., Oojageer, A., Anderson, B., Pizzino, A., Helman, G. *et al.* (2015) Characterization of human disease phenotypes associated with mutations in TREX1, RNASEH2A, RNASEH2B, RNASEH2C, SAMHD1, ADAR, and IFIH1. *Am. J. Med. Genet. A*, **167a**, 296–312.

7. Dyall, S.D., Brown, M.T. and Johnson, P.J. (2004) Ancient Invasions: From Endosymbionts to Organelles. *Science (New York, N.Y.)* **304**, pp. 253–257.

8. Kukat, C., Wurm, C.A., Spahr, H., Falkenberg, M., Larsson, N.G. and Jakobs, S. (2011) Super-resolution microscopy reveals that mammalian mitochondrial nucleoids have a uniform size and frequently contain a single copy of mtDNA. *Proc. Natl. Acad. Sci. USA*, **108**, 13534–13539.

9. Kausar, S., Yang, L., Abbas, M.N., Hu, X., Zhao, Y., Zhu, Y. and Cui, H. (2020) Mitochondrial DNA: a Key regulator of anti-microbial innate immunity. *Genes (Basel)*, **11**:86, 1–22.

10. Cheng, Z., Abrams, S.T., Austin, J., Toh, J., Wang, S.S., Wang, Z., Yu, Q., Yu, W., Toh, C.H. and Wang, G. (2020) The central role and possible mechanisms of bacterial DNAs in sepsis development. *Mediat. Inflamm.*, **2020**, 7418342.

11. Luna-Sánchez, M., Bianchi, P. and Quintana, A. (2021) Mitochondria-induced immune response as a trigger for neurodegeneration: a pathogen from within. *Int. J. Mol. Sci.*, **22**:8523, 1–19.

12. Riley, J.S. and Tait, S.W. (2020) Mitochondrial DNA in inflammation and immunity. *EMBO Rep.*, **21**, e49799.

13. Lepelley, A., Wai, T. and Crow, Y.J. (2021) Mitochondrial nucleic acid as a driver of pathogenic type I interferon induction in Mendelian disease. *Front. Immunol.*, **12**, 729763.

14. Yamazaki, T. and Galluzzi, L. (2022) BAX and BAK dynamics control mitochondrial DNA release during apoptosis. *Cell Death Differ.*, **29**, 1296–1298.

15. Patrushev, M., Kasymov, V., Patrusheva, V., Ushakova, T., Gogvadze, V. and Gaziev, A. (2004) Mitochondrial permeability transition triggers the release of mtDNA fragments. *Cell. Mol. Life Sci.*, **61**, 3100–3103.

16. Kim, J., Gupta, R., Blanco, L.P., Yang, S., Shteinfer-Kuzmine, A., Wang, K., Zhu, J., Yoon, H.E., Wang, X., Kerkhofs, M. *et al.* (2019) VDAC oligomers form mitochondrial pores to release mtDNA fragments and promote lupus-like disease. *Science (New York, N.Y.)*, **366**, 1531–1536.

17. Fang, C., Wei, X. and Wei, Y. (2016) Mitochondrial DNA in the regulation of innate immune responses. *Protein Cell*, **7**, 11–16.

18. Guo, Y., Gu, R., Gan, D., Hu, F., Li, G. and Xu, G. (2020) Mitochondrial DNA drives noncanonical inflammation activation via cGAS-STING signaling pathway in retinal microvascular endothelial cells. *Cell Commun. Signal*, **18**, 172.

19. Huang, L.S., Hong, Z., Wu, W., Xiong, S., Zhong, M., Gao, X., Rehman, J. and Malik, A.B. (2020) mtDNA activates cGAS Signaling and suppresses the YAP-mediated endothelial cell proliferation program to promote inflammatory injury. *Immunity*, **52**, 475–486.e475.

20. Bai, J., Cervantes, C., He, S., He, J., Plasko, G.R., Wen, J., Li, Z., Yin, D., Zhang, C., Liu, M. *et al.* (2020) Mitochondrial stress-activated cGAS-STING pathway inhibits thermogenic program and contributes to overnutrition-induced obesity in mice. *Commun. Biol*, **3**, 257.

21. Decout, A., Katz, J.D., Venkatraman, S. and Ablasser, A. (2021) The cGAS-STING pathway as a therapeutic target in inflammatory diseases. *Nat. Rev. Immunol.*, **21**, 548–569.

22. Dobbs, N., Burnaevskiy, N., Chen, D., Gonugunta, V.K., Alto, N.M. and Yan, N. (2015) STING activation by translocation from the ER is associated with infection and autoinflammatory disease. *Cell Host Microbe.*, **18**, 157–168.

23. West, A.P., Khoury-Hanold, W., Staron, M., Tal, M.C., Pineda, C.M., Lang, S.M., Bestwick, M., Duguay, B.A., Raimundo, N., MacDuff, D.A. *et al.* (2015) Mitochondrial DNA stress primes the antiviral innate immune response. *Nature*, **520**, 553–557.

24. Torres-Odio, S., Lei, Y., Gispert, S., Maletzko, A., Key, J., Menissy, S.S., Wittig, I., Auburger, G. and West, A.P. (2021) Loss of mitochondrial protease CLPP activates type I IFN responses through the mitochondrial DNA-cGAS-STING Signaling Axis. *J. Immunol.*, **206**, 1890–1900.

25. Matsui, H., Ito, J., Matsui, N., Uechi, T., Onodera, O. and Kakita, A. (2021) Cytosolic dsDNA of mitochondrial origin induces cytotoxicity and neurodegeneration in cellular and zebrafish models of Parkinson's disease. *Nat. Commun.*, **12**, 3101.

26. Sliter, D.A., Martinez, J., Hao, L., Chen, X., Sun, N., Fischer, T.D., Burman, J.L., Li, Y., Zhang, Z., Narendra, D.P. *et al.* (2018) Parkin and PINK1 mitigate STING-induced inflammation. *Nature*, **561**, 258–262.

27. Du, S., Chen, G., Yuan, B., Hu, Y., Yang, P., Chen, Y., Zhao, Q., Zhou, J., Fan, J. and Zeng, Z. (2021) DNA sensing and associated type 1 interferon signaling contributes to progression of radiation-induced liver injury. *Cell Mol. Immunol.*, **18**, 1718–1728.

28. Luo, X., Li, H., Ma, L., Zhou, J., Guo, X., Woo, S.L., Pei, Y., Knight, L.R., Deveau, M., Chen, Y. *et al.* (2018) Expression of STING is increased in liver tissues from patients with NAFLD and promotes macrophage-mediated hepatic inflammation and fibrosis in mice. *Gastroenterology*, **155**, 1971–1984.e1974.

29. Thomsen, M.K., Skouboe, M.K., Boularan, C., Vernejoul, F., Lioux, T., Leknes, S.L., Berthelsen, M.F., Riedel, M., Cai, H., Joseph, J.V. *et al.* (2020) The cGAS-STING pathway is a therapeutic target in a preclinical model of hepatocellular carcinoma. *Oncogene*, **39**, 1652–1664.

30. Maekawa, H., Inoue, T., Ouchi, H., Jao, T.M., Inoue, R., Nishi, H., Fujii, R., Ishidate, F., Tanaka, T., Tanaka, Y. *et al.* (2019) Mitochondrial damage causes inflammation via cGAS-STING Signaling in acute kidney injury. *Cell Rep.*, **29**, 1261–1273.e1266.

31. Chung, K.W., Dhillon, P., Huang, S., Sheng, X., Shrestha, R., Qiu, C., Kaufman, B.A., Park, J., Pei, L., Baur, J. *et al.* (2019) Mitochondrial damage and activation of the STING pathway lead to renal inflammation and fibrosis. *Cell Metab.*, **30**, 784–799.e785.

32. Zhao, Q., Wei, Y., Pandol, S.J., Li, L. and Habtezion, A. (2018) STING Signaling promotes inflammation in experimental acute pancreatitis. *Gastroenterology*, **154**, 1822–1835 e1822.

33. Sobek, S. and Boege, F. (2014) DNA topoisomerases in mtDNA maintenance and ageing. *Exp. Gerontol.*, **56**, 135–141.

34. Zhang, H., Barcelo, J.M., Lee, B., Kohlhagen, G., Zimonjic, D.B., Popescu, N.C. and Pommier, Y. (2001) Human mitochondrial topoisomerase I. *Proc. Natl. Acad. Sci. USA*, **98**, 10608–10613.

35. Zhang, X., Li, X.H., Ma, X., Wang, Z.H., Lu, S. and Guo, Y.L. (2006) Redox-induced apoptosis of human oocytes in resting follicles in vitro. *J. Soc. Gynecol. Investig.*, **13**, 451–458.

36. Zhang, H. and Pommier, Y. (2008) Mitochondrial topoisomerase I sites in the regulatory D-loop region of mitochondrial DNA. *Biochemistry*, **47**, 11196–11203.

37. Zhang, H., Zhang, Y.W, Yasukawa, T., Dalla Rosa, I., Khiati, S. and Pommier, Y. (2014) Increased negative supercoiling of mtDNA in TOP1mt knockout mice and presence of topoisomerases II$\alpha$ and II$\beta$ in vertebrate mitochondria. *Nucleic Acids Res.*, **42**, 7259–7267.

38. Sobek, S., Dalla Rosa, I., Pommier, Y., Bornholz, B., Kalfalah, F., Zhang, H., Wiesner, R.J., von Kleist-Retzow, J.C., Hillebrand, F., Schaal, H. *et al.* (2013) Negative regulation of mitochondrial transcription by mitochondrial topoisomerase I. *Nucleic Acids Res.*, **41**, 9848–9857.

39. Al Khatib, I., Deng, J., Symes, A., Kerr, M., Zhang, H., Huang, S.N., Pommier, Y., Khan, A. and Shutt, T.E. (2022) Functional characterization of two variants of mitochondrial topoisomerase TOP1MT that impact regulation of the mitochondrial genome. *J. Biol. Chem.*, **298**, 102420.

40. Han, S., Zhuang, H., Shumyak, S., Yang, L. and Reeves, W.H. (2015) Mechanisms of autoantibody production in systemic lupus erythematosus. *Front. Immunol.*, **6**, 228.

41. Yaniv, G., Twig, G., Shor, D.B., Furer, A., Sherer, Y., Mozes, O., Komisar, O., Slonimsky, E., Klang, E., Lotan, E. *et al.* (2015) A volcanic explosion of autoantibodies in systemic lupus erythematosus: a diversity of 180 different antibodies found in SLE patients. *Autoimmun. Rev.*, **14**, 75–79.

42. Rekvig, O.P. (2015) Anti-dsDNA antibodies as a classification criterion and a diagnostic marker for systemic lupus erythematosus: critical remarks. *Clin. Exp. Immunol.*, **179**, 5–10.

43. Bai, Y., Tong, Y., Liu, Y. and Hu, H. (2018) Self-dsDNA in the pathogenesis of systemic lupus erythematosus. *Clin. Exp. Immunol.*, **191**, 1–10.

44. Fredi, M., Cavazzana, I., Zanola, A., Carabellese, N., Tincani, A., Mahler, M. and Franceschini, F. (2017) Anti-topoisomerase-I antibodies in systemic lupus erythematosus and potential association with the presence of anti-dsDNA antibodies. *Lupus*, **26**, 1121–1122.

45. Stojanov, L., Satoh, M., Dooley, M.A., Kuwana, M., Jennette, J.C. and Reeves, W.H. (1995) Autoantibodies to topoisomerase I in a patient with systemic lupus erythematosus without features of scleroderma. *Lupus*, **4**, 314–317.

46. Hamidou, M.A., Audrain, M.A., Masseau, A., Agard, C. and Moreau, A. (2006) Anti-topoisomerase I antibodies in systemic lupus erythematosus as a marker of severe nephritis. *Clin. Rheumatol.*, **25**, 542–543.

47. Mahler, M., Silverman, E.D., Schulte-Pelkum, J. and Fritzler, M.J. (2010) Anti-Scl-70 (topo-I) antibodies in SLE: myth or reality? *Autoimmun. Rev.*, **9**, 756–760.

48. Budde, P., Zucht, H.D., Vordenbäumen, S., Goehler, H., Fischer-Betz, R., Gamer, M., Marquart, K., Rengers, P., Richter, J., Lueking, A. *et al.* (2016) Multiparametric detection of autoantibodies in systemic lupus erythematosus. *Lupus*, **25**, 812–822.

49. Thim-Uam, A., Prabakaran, T., Tansakul, M., Makjaroen, J., Wongkongkathep, P., Chantaravisoot, N., Saethang, T., Leelahavanichkul, A., Benjachat, T., Paludan, S. *et al.* (2020) STING mediates lupus via the activation of conventional dendritic cell maturation and Plasmacytoid dendritic. *Cell Differentiation, iScience*, **23**, 101530.

50. Li, Y., Wilson, H.L. and Kiss-Toth, E. (2017) Regulating STING in health and disease. *J Inflamm (Lond)*, **14**, 11.

51. Jeremiah, N., Neven, B., Gentili, M., Callebaut, I., Maschalidi, S., Stolzenberg, M.C., Goudin, N., Frémond, M.L., Nitschke, P., Molina, T.J. *et al.* (2014) Inherited STING-activating mutation underlies a familial inflammatory syndrome with lupus-like manifestations. *J. Clin. Invest.*, **124**, 5516–5520.

52. Arneth, B. (2019) Systemic lupus erythematosus and DNA degradation and elimination defects. *Front. Immunol.*, **10**, 1697.

53. Gibson, W.T., Farooqi, I.S., Moreau, M., DePaoli, A.M., Lawrence, E., O'Rahilly, S. and Trussell, R.A. (2004) Congenital leptin deficiency due to homozygosity for the Delta133G mutation: report of another case and evaluation of response to four years of leptin therapy. *J. Clin. Endocrinol. Metab.*, **89**, 4821–4826.

54. Khiati, S., Baechler, S.A., Factor, V.M., Zhang, H., Huang, S.Y., Dalla Rosa, I., Sourbier, C., Neckers, L., Thorgeirsson, S.S. and Pommier, Y. (2015) Lack of mitochondrial topoisomerase I (TOP1mt) impairs liver regeneration. *Proc. Natl. Acad. Sci. USA*, **112**, 11282–11287.

55. Vincent, J., Adura, C., Gao, P., Luz, A., Lama, L., Asano, Y., Okamoto, R., Imaeda, T., Aida, J., Rothamel, K. *et al.* (2017) Small molecule inhibition of cGAS reduces interferon expression in primary macrophages from autoimmune mice. *Nat. Commun.*, **8**, 750.

56. Suter, M.A., Tan, N.Y., Thiam, C.H., Khatoo, M., MacAry, P.A., Angeli, V., Gasser, S. and Zhang, Y.L. (2021) cGAS-STING cytosolic DNA sensing pathway is suppressed by JAK2-STAT3 in tumor cells. *Sci. Rep.*, **11**, 7243.

57. Pépin, G. and Gantier, M.P. (2018) Assessing the cGAS-cGAMP-STING activity of cancer cells. *Methods Mol. Biol. (Clifton, N.J.)*, **1725**, 257–266.

58. Zhang, H., Zhang, Y.W, Yasukawa, T., Dalla Rosa, I., Khiati, S. and Pommier, Y. (2014) Increased negative supercoiling of mtDNA in TOP1mt knockout mice and presence of topoisomerases IIalpha and IIbeta in vertebrate mitochondria. *Nucleic Acids Res.*, **42**, 7259–7267.

59. Yaginuma, K., Kobayashi, M., Taira, M. and Koike, K. (1982) A new RNA polymerase and in vitro transcription of the origin of replication from rat mitochondrial DNA. *Nucleic Acids Res.*, **10**, 7531–7542.

60. Buzan, J.M. and Low, R.L. (1988) Preference of human mitochondrial RNA polymerase for superhelical templates with mitochondrial promoters. *Biochem. Biophys. Res. Commun.*, **152**, 22–29.

61. Fukuoh, A., Ohgaki, K., Hatae, H., Kuraoka, I., Aoki, Y., Uchiumi, T., Jacobs, H.T. and Kang, D. (2009) DNA conformation-dependent activities of human mitochondrial RNA polymerase. *Genes Cells*, **14**, 1029–1042.

62. Barat-Gueride, M., Dufresne, C. and Rickwood, D. (1989) Effect of DNA conformation on the transcription of mitochondrial DNA. *Eur. J. Biochem.*, **183**, 297–302.

63. Zollo, O. and Sondheimer, N. (2017) Topological requirements of the mitochondrial heavy-strand promoters. *Transcription*, **8**, 307–312.

64. Tang, J.X., Thompson, K., Taylor, R.W. and Oláhová, M. (2020) Mitochondrial OXPHOS biogenesis: co-regulation of protein synthesis, import, and assembly pathways. *Int. J. Mol. Sci.*, **21**:3820, 1–32.

65. Baechler, S.A., Factor, V.M., Dalla Rosa, I., Ravji, A., Becker, D., Khiati, S., Miller Jenkins, L.M., Lang, M., Sourbier, C., Michaels, S.A. *et al.* (2019) The mitochondrial type IB topoisomerase drives mitochondrial translation and carcinogenesis. *Nat. Commun.*, **10**, 83.

66. Taguchi, T., Mukai, K., Takaya, E. and Shindo, R. (2021) STING operation at the ER/Golgi Interface. *Front. Immunol.*, **12**, 646304.

67. Khiati, S., Dalla Rosa, I., Sourbier, C., Ma, X., Rao, V.A., Neckers, L.M., Zhang, H. and Pommier, Y. (2014) Mitochondrial topoisomerase I (top1mt) is a novel limiting factor of doxorubicin cardiotoxicity. *Clin. Cancer Res.*, **20**, 4873–4881.

68. Zhang, H., Seol, Y., Agama, K., Neuman, K.C. and Pommier, Y. (2017) Distribution bias and biochemical characterization of TOP1MT single nucleotide variants. *Sci. Rep.*, **7**, 8614.

69. Wang, W., Shen, P., Thiyagarajan, S., Lin, S., Palm, C., Horvath, R., Klopstock, T., Cutler, D., Pique, L., Schrijver, I. *et al.* (2011) Identification of rare DNA variants in mitochondrial disorders with improved array-based sequencing. *Nucleic Acids Res.*, **39**, 44–58.

70. Lei, Y., Guerra Martinez, C., Torres-Odio, S., Bell, S.L., Birdwell, C.E., Bryant, J.D., Tong, C.W., Watson, R.O., West, L.C. and West, A.P. (2021) Elevated type I interferon responses potentiate metabolic dysfunction, inflammation, and accelerated aging in mtDNA mutator mice. *Sci. Adv.*, **7**:eabe7548, 1–16.

71. Lepelley, A., Della Mina, E., Van Nieuwenhove, E., Waumans, L., Fraitag, S., Rice, G.I., Dhir, A., Frémond, M.L., Rodero, M.P., Seabra, L. *et al.* (2021) Enhanced cGAS-STING-dependent interferon signaling associated with mutations in ATAD3A. *J. Exp. Med.*, **218**:e20201560, 1–18.

72. Kamen, D.L. (2014) Environmental influences on systemic lupus erythematosus expression. *Rheum. Dis. Clin. N. Am.*, **40**, 401–412, vii.

73. Perl, A. (2010) Pathogenic mechanisms in systemic lupus erythematosus. *Autoimmunity*, **43**, 1–6.

74. Lood, C., Blanco, L.P., Purmalek, M.M., Carmona-Rivera, C., De Ravin, S.S., Smith, C.K., Malech, H.L., Ledbetter, J.A., Elkon, K.B. and Kaplan, M.J. (2016) Neutrophil extracellular traps enriched in oxidized mitochondrial DNA are interferogenic and contribute to lupus-like disease. *Nat. Med.*, **22**, 146–153.

75. Leishangthem, B.D., Sharma, A. and Bhatnagar, A. (2016) Role of altered mitochondria functions in the pathogenesis of systemic lupus erythematosus. *Lupus*, **25**, 272–281.

76. An, J., Durcan, L., Karr, R.M., Briggs, T.A., Rice, G.I., Teal, T.H., Woodward, J.J. and Elkon, K.B. (2017) Expression of cyclic GMP-AMP synthase in patients with systemic lupus erythematosus. *Arthritis Rheumatol*, **69**, 800–807.

77. Kato, Y., Park, J., Takamatsu, H., Konaka, H., Aoki, W., Aburaya, S., Ueda, M., Nishide, M., Koyama, S., Hayama, Y. *et al.* (2018) Apoptosis-derived membrane vesicles drive the cGAS-STING pathway and enhance type I IFN production in systemic lupus erythematosus. *Ann. Rheum. Dis.*, **77**, 1507–1515.

78. Meas, R., Burak, M.J. and Sweasy, J.B. (2017) DNA repair and systemic lupus erythematosus. *DNA Repair (Amst)*, **56**, 174–182.

79. Sallai, K., Nagy, E., Derfalvy, B., Müzes, G. and Gergely, P. (2005) Antinucleosome antibodies and decreased deoxyribonuclease activity in sera of patients with systemic lupus erythematosus. *Clin. Diagn. Lab. Immunol.*, **12**, 56–59.

80. Yasutomo, K., Horiuchi, T., Kagami, S., Tsukamoto, H., Hashimura, C., Urushihara, M. and Kuroda, Y. (2001) Mutation of DNASE1 in people with systemic lupus erythematosus. *Nat. Genet.*, **28**, 313–314.

81. Al-Mayouf, S.M., Sunker, A., Abdwani, R., Abrawi, S.A., Almurshedi, F., Alhashmi, N., Al Sonbul, A., Sewairi, W., Qari, A., Abdallah, E. *et al.* (2011) Loss-of-function variant in DNASE1L3 causes a familial form of systemic lupus erythematosus. *Nat. Genet.*, **43**, 1186–1188.

82. Zervou, M.I., Andreou, A., Matalliotakis, M., Spandidos, D.A., Goulielmos, G.N. and Eliopoulos, E.E. (2020) Association of the DNASE1L3 rs35677470 polymorphism with systemic lupus erythematosus, rheumatoid arthritis and systemic sclerosis: structural biological insights. *Mol. Med. Rep.*, **22**, 4492–4498.

83. Lee-Kirsch, M.A., Gong, M., Chowdhury, D., Senenko, L., Engel, K., Lee, Y.A., de Silva, U., Bailey, S.L., Witte, T., Vyse, T.J. *et al.* (2007) Mutations in the gene encoding the 3′-5′ DNA exonuclease TREX1 are associated with systemic lupus erythematosus. *Nat. Genet.*, **39**, 1065–1067.

84. Fye, J.M., Orebaugh, C.D., Coffin, S.R., Hollis, T. and Perrino, F.W. (2011) Dominant mutation of the TREX1 exonuclease gene in lupus and Aicardi-Goutieres syndrome. *J. Biol. Chem.*, **286**, 32373–32382.

85. López-López, L., Nieves-Plaza, M., Castro Mdel, R., Font, Y.M., Torres-Ramos, C.A., Vilá, L.M. and Ayala-Peña, S. (2014) Mitochondrial DNA damage is associated with damage accrual and disease duration in patients with systemic lupus erythematosus. *Lupus*, **23**, 1133–1141.

86. Goffart, S., Hangas, A. and Pohjoismaki, J.L.O. (2019) Twist and turn-topoisomerase functions in mitochondrial DNA maintenance. *Int. J. Mol. Sci.*, **20**:2041, 1–17.

87. Douarre, C., Sourbier, C., Dalla Rosa, I., Brata Das, B., Redon, C.E., Zhang, H., Neckers, L. and Pommier, Y. (2012) Mitochondrial topoisomerase I is critical for mitochondrial integrity and cellular energy metabolism. *PLoS One*, **7**, e41094.

88. Piccinini, G., Cardellini, E., Reimer, G., Arnett, F.C. and Durban, E. (1991) An antigenic region of topoisomerase I in DNA polymerase chain reaction-generated fragments recognized by autoantibodies of scleroderma patients. *Mol. Immunol.*, **28**, 333–339.

89. Hongliang Zhang, M.K. and Pommier, Y. Using mitochondrial TOP1 (TOP1mt) to probe the involvement of mitochondria in systemic lupus erythematosus. Virtual Keystone Symposia .

90. Dalla Rosa, I., Huang, S.Y., Agama, K., Khiati, S., Zhang, H. and Pommier, Y. (2014) Mapping topoisomerase sites in mitochondrial DNA with a poisonous mitochondrial topoisomerase I (Top1mt). *J. Biol. Chem.*, **289**, 18595–18602.

91. Wu, Z., Oeck, S., West, A.P., Mangalhara, K.C., Sainz, A.G., Newman, L.E., Zhang, X.O., Wu, L., Yan, Q., Bosenberg, M. *et al.* (2019) Mitochondrial DNA stress signalling protects the nuclear genome. *Nat Metab*, **1**, 1209–1218.

92. Jiang, M., Chen, P., Wang, L., Li, W., Chen, B., Liu, Y., Wang, H., Zhao, S., Ye, L., He, Y. *et al.* (2020) cGAS-STING, an important pathway in cancer immunotherapy. *J. Hematol. Oncol.*, **13**, 81.

93. Sabouny, R., Wong, R., Lee-Glover, L., Greenway, S.C., Sinasac, D.S., Khan, A. and Shutt, T.E. (2019) Characterization of the C584R variant in the mtDNA depletion syndrome gene FBXL4, reveals a novel role for FBXL4 as a regulator of mitochondrial fusion. *Biochim. Biophys. Acta Mol. basis Dis.*, **1865**, 165536.

94. Newman, L.E., Tadepalle, N., Novak, S.W., Schiavon, C.R., Rojas, G.R., Chevez, J.A., Lemersal, I., Medina, M., Rocha, S., Towers, C.G. *et al.* (2022) Endosomal removal and disposal

of dysfunctional, immunostimulatory mitochondrial DNA. *bioRxiv*, 2022.2010.2012.511955. print:https://www.biorxiv.org/content/10.1101/2022.10.12.511955v1.

95. Chatre, L.R.M. (2015) *Mitochondrial medicine*. In Edeas, V.W.M. (ed), *Probing Mitochondrial Function*. Vol. I, Springer, New York, pp. 133–147.

96. Donkervoort, S., Sabouny, R., Yun, P., Gauquelin, L., Chao, K.R., Hu, Y., Al Khatib, I., Töpf, A., Mohassel, P., Cummings, B.B. *et al.* (2019) MSTO1 mutations cause mtDNA depletion, manifesting as muscular dystrophy with cerebellar involvement. *Acta Neuropathol.*, **138**, 1013–1031.

97. Eaton, J.S., Lin, Z.P., Sartorelli, A.C., Bonawitz, N.D. and Shadel, G.S. (2007) Ataxia-telangiectasia mutated kinase regulates ribonucleotide reductase and mitochondrial homeostasis. *J. Clin. Invest.*, **117**, 2723–2734.

98. Baek, M., DiMaio, F., Anishchenko, I., Dauparas, J., Ovchinnikov, S., Lee, G.R., Wang, J., Cong, Q., Kinch, L.N., Schaeffer, R.D. *et al.* (2021) Accurate prediction of protein structures and interactions using a three-track neural network. *Science (New York, N.Y.)*, **373**, 871–876.

99. van Zundert, G.C.P., Rodrigues, J., Trellet, M., Schmitz, C., Kastritis, P.L., Karaca, E., Melquiond, A.S.J., van Dijk, M., de Vries, S.J. and Bonvin, A. (2016) The HADDOCK2.2 web server: user-friendly integrative Modeling of biomolecular complexes. *J. Mol. Biol.*, **428**, 720–725.

100. Honorato, R.V., Koukos, P.I., Jiménez-García, B., Tsaregorodtsev, A., Verlato, M., Giachetti, A., Rosato, A. and Bonvin, A. (2021) Structural biology in the clouds: the WeNMR-EOSC ecosystem. *Front. Mol. Biosci.*, **8**, 729513.

101. Baker, N.A., Sept, D., Joseph, S., Holst, M.J. and McCammon, J.A. (2001) Electrostatics of nanosystems: application to microtubules and the ribosome. *Proc. Natl. Acad. Sci. USA*, **98**, 10037–10041.